Multicomponent Kardar-Parisi-Zhang Universality in Degenerate Coupled Condensates Supplemental Materials

Harvey Weinberger[1], Paolo Comaron[1,2], and Marzena H. Szymańska[1]
[1]Department of Physics and Astronomy, University College London, Gower Street, London, WC1E 6BT, United Kingdom and
[2]CNR NANOTEC, Institute of Nanotechnology, Via Monteroni, 73100 Lecce, Italy

In this supplemental material, we outline the Wilsonian renormalisation group procedure for the multicomponent degenerate KPZ equations and other numerical methods used to produce the results presented in the main manuscript. The material is divided into six Supplementary Notes: (S1) The derivation of the multicomponent $\mathbb{Z}_2$ KPZ equation from Keldysh field theory and discussion around its stability (S2) Properties of the multicomponent KPZ equation, particularly its adimensionalised form and conditions for a stationary measure (S3) Derivation and discussion of the Wilsonian RG procedure from the MSRJD functional integral, along with subsequent discussion of the flow equations (S4) Direct numerical integration of the KPZ equation and comparison with Tracy-Widom GOE distributions including additional simulations of the (X, Y)-plane in FIG. 2 (S5) Direct numerical integration of the SCGLE, focusing on compact features such as spacetime vortices proliferating in the instability regime in Quadrant IV (S6) Discussion of the mapping from the generalised Gross-Pitaevskii Equations with multicomponent exciton cavity and parameter plots in the (X, Y)-plane.

SUPPLEMENTARY NOTE 1 : WEAKLY INTERACTING DRIVEN-DISSIPATIVE CONDENSATES

In this section, we derive the effective theory for the Nambu-Goldstone (NG) modes of the $\mathbb{Z}_2$ coupled condensate under drive and dissipation using the Lindbladian formalism and Keldysh field theory. Starting from the Lindbladian, we motivate the SCGLE as a semiclassical description of a quantum model suitable for weakly-interacting bosons at mesoscopic scales.

Schwinger-Keldysh Partition Function and Semiclassical Action

In this section, we explain how systems of interacting bosons with drive and disspation can be mapped to the Schwinger-Keldysh path integral describing the evolution of the reduced density matrix describing the lower polariton bands $\psi_{LP,\sigma}$ with polarisation degree of freedom. Exciton-polariton systems are formed from strong coupling between cavity photons, trapped between Bragg mirrors forming a microcavity, and Wannier-Mott excitons. The exciton has two bright states with spin projection $J_z = \{-1, +1\}$ which couple to the photonic components giving rise to a multicomponent structure due to the polarisation. We assume that the effective Hamiltonian governing the coherent dynamics of the lower polariton bands is

$$\hat{H}_{LP} = \int_x \left[\sum_\sigma \left[\hat{\Psi}^\dagger_\sigma \left(-k_c \partial_x^2 + \mu_c\right) \hat{\Psi}_\sigma)\right) + u_c \hat{\Psi}^\dagger_\sigma \hat{\Psi}^\dagger_\sigma \hat{\Psi}_\sigma \hat{\Psi}_\sigma \right] + \sum_{\sigma \neq \sigma'} \left[v_c \hat{\Psi}^\dagger_\sigma \hat{\Psi}^\dagger_{\sigma'} \hat{\Psi}_{\sigma'} \hat{\Psi}_\sigma \right] \right] \tag{S.1}$$

where $\int_x = \int dx$ and the sum is over polarisation states which are indexed $\{1, 2\}$ in the main paper. The interaction stems from various mechanisms but predominantly originates from screened Coulombic interactions between excitons, formed from holes and electrons. In the low-energy scattering regime for the lower-polariton band, the interactions are local contact intracomponent u_c and intercomponent v_c 4-point density-density interactions. The operators are bosonic and obey the same-time algebraic structure

$$[\hat{\Psi}_\sigma(x, t), \hat{\Psi}^\dagger_{\sigma'}(x', t)] = \delta_{\sigma\sigma'} \delta(x - x')\,, \quad [\hat{\Psi}_\sigma(x, t), \hat{\Psi}_{\sigma'}(x', t)] = 0. \tag{S.2}$$

The central feature of our model is the additional requirement of a $\mathbb{Z}_2$ symmetry, requiring invariance under inversions in field space $\hat{\Psi}_1 \leftrightarrow \hat{\Psi}_2$. As explained in the main text, this arises in samples with small transverse-electric transverse magnetic splitting and with equal polarisation pumping schemes. However, in addition to coherent dynamics, the polaritons are also driven-dissipative and require pumping from a laser to compensate for cavity losses. We assume that these losses can be modelled by the polariton bands interacting with a Markovian environment. The dynamics of the reduced density matrix $\hat{\rho}$ is then governed by a Lindblad master equation

$$\partial_t \hat{\rho} = -i[\hat{H}_{LP}, \hat{\rho}] + \sum_\alpha \gamma_\alpha \left[\hat{L}_\alpha \hat{\rho} \hat{L}^\dagger_\alpha - \frac{1}{2} \left\{ \hat{L}^\dagger_\alpha \hat{L}_\alpha,\, \hat{\rho} \right\} \right] \tag{S.3}$$

with Lindblad operators with homogeneous coupling constants γ_α (i) single particle pumping from lasing $\hat{\Psi}_i^\dagger$ proportional to γ_p (ii) single particle losses $\hat{\Psi}_i$ proportional to γ_l (iii) two particle non-linear losses $\hat{\Psi}_i\hat{\Psi}_i$ proportional to $2u_d$ (iv) cross-component two particle non-linear losses $(\hat{\Psi}_1\hat{\Psi}_2 + \hat{\Psi}_2\hat{\Psi}_1)$ proportional to $2v_d$ and (v) momentum dependent losses from an operator of the form $\hat{p}\hat{\Psi}$ which generate terms proportional to $(\partial_x \hat{\Psi}_{i,x})$ since the operators are expressed in the position basis with coupling constant equal to $2k_d$. This choice of Lindblad operators preserves the $U(1)\times U(1)$ symmetry of the action, ensuring that the low-energy sector is described by two coupled NG modes. In equilibrium zero-temperature QFTs, we are typically concerned with calculating time-ordered expectations of operators in the ground state $|\Omega\rangle$. Non-equilibrium QFTs, such as Keldysh field theory, share a similar structure but now instead of working with states $|i\rangle$, the theory focuses on the dynamical evolution of density matrices $\hat{\rho}$. The fundamental object in Schwinger-Keldysh theories is the partition function

$$\mathcal{Z} = \mathrm{Tr}[e^{\hat{\mathcal{L}}t}[\hat{\rho}(t_0)]] = 1\,. \tag{S.4}$$

The partition function is exactly unity in the absence of sources reflecting conservation of probability along dynamics generated by the Lindbladian operator which is a completely positive trace-preserving map. To derive the mesoscopic Eq. (1), we use the dynamical semigroup property of the Lindbladian and the Schwinger-Keldysh closed loop formalism. The real-time field theory is constructed by resolving coherent states in Trotter steps which are constructed to satisfy

$$\int \prod_\sigma \left(\frac{d\psi_{\sigma,t_n} d\bar{\psi}_{\sigma,t_n}}{\pi}\right) e^{-\sum_\sigma |\psi_{\sigma,t_n}|^2} |\Psi_{\sigma,t_n}\rangle\langle\Psi_{\sigma,t_n}| = \mathbb{1}, \quad \langle\Psi_{\sigma,t_l}|\Psi_{\sigma,t_m}\rangle = e^{\bar{\psi}_{\sigma,t_l}\psi_{\sigma,t_m}} \tag{S.5}$$

where the operators are indexed by t_n on the forward and backward contour. The field operators have action on coherent states:

$$\hat{\Psi}_\sigma |\Psi_{\sigma,t_n}\rangle = \psi_{\sigma,t_n} |\Psi_{\sigma,t_n}\rangle \;\; \text{with} \;\; \psi_{\sigma,t_n} \in \mathbb{C}. \tag{S.6}$$

Since the Hamiltonian is normal ordered, the resolution of identity via trotterisation is trivial and the partition function can be mapped to a coherent state path integral upon taking the mesh trotterisation to zero. There is an additional complication with the normal ordering of the pump term as the Lindblad operator reads $\hat{L}^\dagger L = \Psi_\sigma \Psi_\sigma^\dagger$, but this can be dealt with appropriately as done in Ref. [1]. There is a doubling of the field degrees of freedom and truly non-equilibrium dynamics arises from couplings between fields on the forward contour C_+ running along the real axis in the complex time plane from $t_0 = -\infty$ to $t_f = \infty$ and the backward contour C_-. Since we are interested in the long-time stationary dynamics, we can extend the integral from $t_0 = -\infty$ to $t_f = \infty$ and given the driven-dissipative nature and irreducibility, the long time dynamics should flow to a unique stationary state of the Lindbladian irrespective of the initial condition, allowing us to ignore the boundary condition at t_0. In the semiclassical limit which is justified in the vicinity of a phase transition, terms greater than $\mathcal{O}((\psi^q)^2)$ are ignored, which allows for the original partition function in Eq.(S.4) to be restated as

$$\mathcal{Z} = \int \mathcal{D}[\psi_i^c, \psi_i^q]\; e^{i\mathcal{S}[\psi_i^c,\psi_i^q]} \tag{S.7}$$

with effective microscopic action

$$\begin{aligned}\mathcal{S} = \int_{x,t} &\left(\left[\bar{\psi}_i^q \left(i\partial_t + k\partial_x^2 - \mu\right)\psi_i^c\right] - u\left[\bar{\psi}_i^q\bar{\psi}_i^c\psi_i^c\psi_i^c\right] - v\left[\bar{\psi}_1^c\psi_1^c\bar{\psi}_2^q\psi_2^c + (1\leftrightarrow 2)\right] + \text{c.c.}\right) \\ &+ 4iu_d\bar{\psi}_i^c\psi_i^c\bar{\psi}_i^q\psi_i^q + 2iv_d\left[\bar{\psi}_2^c\psi_2^c\bar{\psi}_1^q\psi_1^q + \bar{\psi}_1^c\psi_2^c\bar{\psi}_2^q\psi_1^q + (1\leftrightarrow 2)\right] + 2i\gamma_t\bar{\psi}_i^q\psi_i^q + ik_d(\partial_x\overline{\psi}_i^q)(\partial_x\psi_i^q)\end{aligned} \tag{S.8}$$

where $k = k_c - ik_d$, $\mu = \mu_c + i\mu_d$, $u = u_c - iu_d$, $v = v_c - iv_d$ with free indices implicitly summed over. In the original Lindblad parameters, $\mu_d = (\gamma_p - \gamma_l)/2$ and $\gamma_T = (\gamma_p + \gamma_l)/2$. There is also a momentum dependent term in the $q - q$ coupling which is dropped as it is subleading and does not contribute to the low-energy theory. When the lasing gain γ_p exceeds the single particle losses γ_l to the reservoir of uncondensed particles, spontaneous symmetry breaking (SSB) of the $U(1)\times U(1)$ symmetry occurs. This results in a finite expectation value for the classical fields $\langle\psi_\sigma^c\rangle \neq 0$. Since the theory is Gaussian in the quantum fields, auxiliary white noise fields $\zeta_i \in \mathbb{C}$ can be introduced via the Hubbard-Stratonovich transformation. After integrating out quantum fields and absorbing constants into the functional measure, we obtain the SCGLE:

$$i\partial_t\psi_i = \Big[-(k_c - ik_d)\partial_x^2 + (\mu_c + i\mu_d) + (u_c - iu_d)|\psi_i|^2 + (v_c - iv_d)|\psi_{\bar{i}}|^2\Big]\psi_i + \zeta_i. \tag{S.9}$$

However, there is an ambiguity in the form of the noise covariance for Eq. (1) as including density contributions in the action in Eq.(S.8) from terms quadratic in ψ_i^q gives:

$$\langle \zeta_i^*(x,t)\zeta_j(x',t')\rangle = \begin{pmatrix} 2((2|\psi_1^c|^2 u_d + |\psi_2^c|^2 v_d) + \gamma_T) & 2\bar{\psi}_2^c \psi_1^c v_d \\ 2\bar{\psi}_1^c \psi_2^c v_d & 2((2|\psi_2^c|^2 u_d + |\psi_1^c|^2 v_d) + \gamma_T) \end{pmatrix}_{ij} \delta(x-x')\,\delta(t-t'). \tag{S.10}$$

where there is an additional non-trivial covariance between the white noise driving the individual field components. For the direct integration of the SCGLE in FIG. 1(b) and analysis of the onset of spacetime vortices detailed in Section E, we assume that the noise is an additive constant with subleading density corrections. In this approximation, the covariance becomes diagonal and equal to $2\gamma_T$ giving Eq. (1).

Diffusive NG Modes Stability

We can analyse the stability of the condensate to small fluctuations by expanding the action in Eq. (S.8) in Nambu fluctuations around the mean field. The eigenspectra of the modes is encoded by the poles of the retarded Green's function G^R which inherits a 4×4 matrix structure. Equivalent insight can be gained starting from the SCGLE. Ignoring the additive white noise, we can derive Eq. (2) for the stability of the Bogoliubov fluctuations around a homogeneous mean field. In the SSB phase, fluctuations around the mean field $\rho = |\psi_i^{(0)}|^2$ can be considered. Guided by the coset construction, the density-phase representation parameterisation

$$\psi_i = \sqrt{\rho + \chi_i(x,t)}\, e^{i(\theta_{i,0} + \theta_i(x,t))} \tag{S.11}$$

will correctly capture the low-energy theory where $\theta_{i,0}$, θ_i, ρ, $\chi_i \in \mathbb{R}$. Inserting the ansatz into Eq. (1) and considering terms up to linear order in fluctuations gives the equation

$$\partial_t \begin{pmatrix} \chi_1 \\ \theta_1 \\ \chi_2 \\ \theta_2 \end{pmatrix} = \begin{pmatrix} k_d\partial_x^2 - 2\rho u_d & -2\rho k_c \partial_x^2 & -2\rho v_d & 0 \\ -k_c\partial_x^2 + 2\rho u_c & -2\rho k_d \partial_x^2 & 2\rho v_c & 0 \\ -2\rho v_d & 0 & k_d\partial_x^2 - 2\rho u_d & -2\rho k_c \partial_x^2 \\ 2\rho v_c & 0 & -k_c\partial_x^2 + 2\rho u_c & -2\rho k_d \partial_x^2 \end{pmatrix} \begin{pmatrix} \chi_1 \\ \theta_1 \\ \chi_2 \\ \theta_2 \end{pmatrix}. \tag{S.12}$$

We define the Fourier transform convention

$$\theta^\alpha(x,t) = \int_{k,\omega} \theta^\alpha_{\omega,k} e^{-i\omega t + ik\cdot x} \tag{S.13}$$

with integration measure $d\omega\, dk/(2\pi)^2$. Transforming to the Fourier representation gives a linear equation $-i\omega\Psi = M\Psi$. The eigenspectra can then be found from solving a quartic,

$$\begin{aligned} \omega_{\chi,\pm} &= -i\rho(u_d \pm v_d) - ik_d k^2 - \sqrt{(k_c k^2)^2 + 2k_c k^2 \rho(u_c \pm v_c) - (u_d \pm v_d)^2\rho^2} \\ \omega_{\theta,\pm} &= -i\rho(u_d \pm v_d) - ik_d k^2 + \sqrt{(k_c k^2)^2 + 2k_c k^2 \rho(u_c \pm v_c) - (u_d \pm v_d)^2\rho^2}. \end{aligned} \tag{S.14}$$

We plot the spectra for the cases considered in FIG. 1(a-c) in FIG. S1 directly showing that for parameters in Quadrants II and III, regions of the imaginary parts of the spectrum lie in the upper half-plane. For stability, fluctuations must decay, which requires that all eigenvalues lie in the lower half-complex plane. Considering a low-momentum expansion up to order $O(k^2)$, the eigenvalues are

$$\begin{aligned} \omega_{\chi,\pm} &= -i\left[2\rho(u_d \pm v_d) - k^2\left(k_c \frac{u_c \pm v_c}{u_d \pm v_d} - k_d\right)\right] \\ \omega_{\theta,\pm} &= -ik^2\left(k_c \frac{u_c \pm v_c}{u_d \pm v_d} + k_d\right). \end{aligned} \tag{S.15}$$

and these can be used to give a condition which generalises the condition in Ref.[2] as we additionally have a bound from below. As $k \to 0$, $\omega_{\chi,\pm}$ has finite damping. This procedure reveals two gapped density modes and two NG diffusive modes, unlike the equilibrium case. For zeroth order stability, $u_d - v_d > 0 \implies \tilde{v}_d = v_d/u_d < 1$; the intercomponent non-linear dissipative term is bounded by the intracomponent non-linear dissipative term. If this condition is violated, the gapped modes become unstable and drive a dynamical phase transition. Stability of the gapless modes while in the regime $u_d - v_d > 0$ imposes that both

$$(k_c(u_c + v_c) + k_d(u_d + v_d)) > 0 \text{ and } (k_c(u_c - v_c) + k_d(u_d - v_d)) > 0 \tag{S.16}$$

are satisfied. Assuming that we are both in the positive mass regime, $k_c > 0$, and the intracomponent interaction is repulsive $u_c > 0$, gives Eq. (2)

$$-1 - \mathcal{R}(u)\mathcal{R}(k)(1+\tilde{v}_d) < \tilde{v}_c < 1 + \mathcal{R}(u)\mathcal{R}(k)(1-\tilde{v}_d) \tag{S.17}$$

where $\mathcal{R}(k) = k_d/k_c$ and $\tilde{v}_c = v_c/u_c$. Approaching the equilibrium limit $R(k) \to 0$, $R(u) \to 0$, $\tilde{v}_d \to 0$ recovers the more restrictive equilibrium condition $-1 < \tilde{v}_c < 1$ and the four modes become gapless. This means that non-equilibrium condensates are more stable against gapless diffusive fluctuations. In Quadrants II and III in FIG. 2, Eq. (2) is not satisfied and this drives a dynamical phase transition and subsequent fragmentation of the condensate. An equivalent formulation of Eq. (2) can be obtained by demanding that the diffusion matrix for the mapped KPZ effective equation is positive-definite. Instead of analysing the small momentum $O(k^2)$ expansion, we can also understand the stability by appealing to the Routh-Hurwitz stability condition which determines whether a linear system of equations have only stable solutions. Starting from the eigenspectrum condition $\det[-i\omega - M] = 0$, we get a quartic which factorises into two quadratics

$$\begin{aligned}\left[\tilde{\omega}^2 + 2\tilde{\omega}\left(k^2 k_d + (u_d - v_d)\rho\right) + k^4(k_c^2 + k_d^2) + 2\rho k^2(k_c(u_c - v_c) + k_d(u_d - v_d))\right] = 0\\ \left[\tilde{\omega}^2 + 2\tilde{\omega}\left(k^2 k_d + (u_d + v_d)\rho\right) + k^4(k_c^2 + k_d^2) + 2\rho k^2(k_c(u_c + v_c) + k_d(u_d + v_d))\right] = 0\end{aligned} \tag{S.18}$$

where we additionally defined $\tilde{\omega} = -i\omega$. For a second order polynomial $P(s) = a_2 s^2 + a_1 s + a_0$, the stability condition states that the system is stable if and only if $a_0,\ a_1,\ a_2 > 0$. This means that for $u_d,\ v_d,\ k_d > 0$, then $a_1 > 0$ gives the zeroth order stability condition $u_d > v_d$. Requiring that $a_0 > 0$ for all momentum k to $O(k^2)$ recovers the conditions in Eq. (S.16). In general, the condition $a_0 > 0$, guaranteeing the stability of a given momentum mode k, is

$$k^2\left[2\rho\left(k_c(u_c \pm v_c) + k_d(u_d \pm v_d)\right) + (k_c^2 + k_d^2)k^2\right] > 0\,. \tag{S.19}$$

For $k \neq 0$, this condition can be rearranged to give a condition on $\tilde{v}_c$ assuming $k_c,\ \rho,\ u_c > 0$

$$-1 - R(u)R(k)(1+\tilde{v}_d) - \frac{k_c k^2}{2u_c\rho}(1+\mathcal{R}(k)^2) < \tilde{v}_c < 1 + R(u)R(k)(1-\tilde{v}_d) + \frac{k_c k^2}{2u_c\rho}(1+\mathcal{R}(k)^2). \tag{S.20}$$

Requiring that this is true for all k, including $k = 0$, gives the condition Eq. (2). Strictly, the zero-momentum mode for the gapless fluctuations critically fails the Routh-Kurwitz test.

Low Energy Effective Field Theory

The low-energy sector dynamics is described by the multicomponent KPZ Eq. (3) for the phase fluctuations. We derive the effective equations starting from the semiclassical partition function with action in Eq. (S.8). The action is written in the rotated Keldysh coordinates for classical and quantum fields, however due to couplings of fields lying on forward and backward contours in Action (S.8), the symmetries along the forward and backward contours are explicitly broken down to the diagonal subgroup $U(1) \times U(1)$ with the complex fields mapping to

$$\psi_i^c \mapsto e^{i\theta_i}\psi_i^c, \quad \psi_i^q \mapsto e^{i\theta_i}\psi_i^q \tag{S.21}$$

where the i subscripts run over the spinor indices. This corresponds to joint phase rotations between the classical and quantum fields. This weak symmetry also generates a variant of the classical Noether's theorem which states that the unphysical quantum current $j^\mu_{i,q}$ for each component is conserved with $\langle \partial_\mu j^\mu_{i,q}\rangle = 0$ where $j^0_{i,q} = \overline{\psi}_{i,c}\psi_{i,q} + \overline{\psi}_{i,q}\psi_{i,c}$. In the condensed phase $\rho > 0$, the NG modes are parameterised $\psi_i^c = \sqrt{\rho_i}e^{i\theta_i}$ and $\psi_i^q = (\xi_i^R + i\xi_i^I)e^{i\theta_i}$. The Jacobian of this coordinate transformation is absorbed into the path integral measure since it is field independent and poses no issues for $\rho_i > 0$. The new fields have target spaces: the entire $\mathbb{R}$ line for $\xi_i^{R/I}$, $\mathbb{R}^+ \setminus 0$ for ρ_i, and the space $[0, 2\pi]$ for θ_i. Integrating out gapped density fluctuations around a strong mean field leads to the effective field theory describing the low-energy sector. The mean field solution is valid for weakly-interacting bosons in the condensed phase where fluctuations are small. The low-energy partition function is given by

$$\mathcal{Z} = \int \mathcal{D}[\rho_i, \xi_i^R, \xi_i^I, \theta_i]\; e^{i\left(S^R[\rho_i,\xi_i^R,\xi_i^I,\theta_i] + iS^I[\rho_i,\xi_i^R,\xi_i^I,\theta_i]\right)} \tag{S.22}$$

where S_R can be found by substituting the NG mode parameterisation. Terms quadratic in quantum fields give rise to the imaginary part of the action,

$$S^I = \int_{x,t} 2(2\rho_1 u_d + \rho_2 v_d + \gamma_T)\left[(\xi_1^R)^2 + (\xi_1^I)^2\right] + (8\sqrt{\rho_1}\sqrt{\rho_2}v_d)\left[\xi_1^R\xi_2^R + \xi_1^I\xi_2^I\right] + 1 \leftrightarrow 2. \tag{S.23}$$

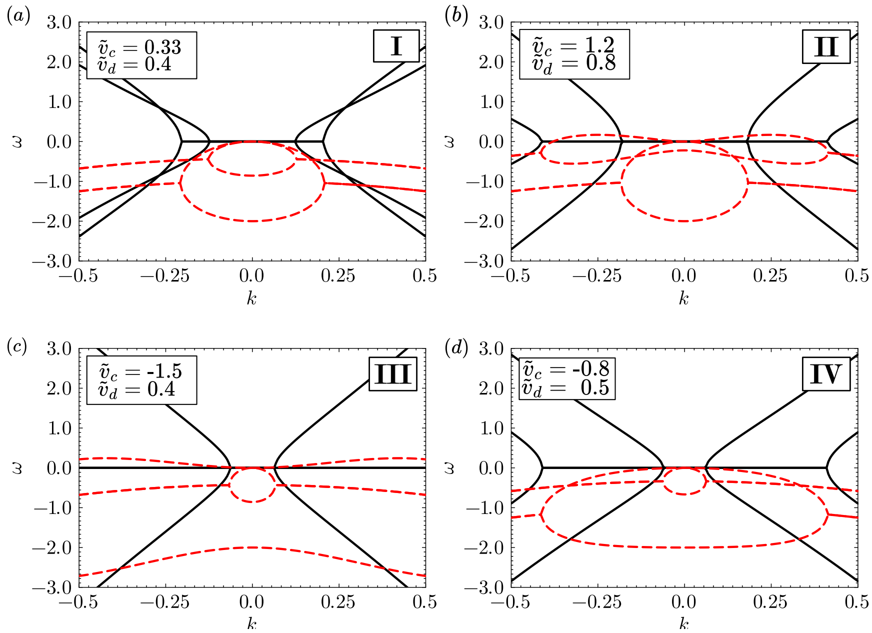

FIG. S1. **Bogoliubov Spectra for Coupled Driven Condensates** : (a-d) showing the full Bogoliubov spectra from Eq. (S.14) for parameters in Quadrants I-IV in FIG. 1. The spectra use parameters $\mu_d = u_d = k_d = 1$, $u_c = 3$, $k_c = 4$. The red line shows the imaginary part of the spectra revealing gapless diffusive modes and the real part of the spectra is shown in black. If $\mathrm{Im}[\omega] > 0$, the system develops an instability leading to large density fluctuations. Quadrants I and IV are stable for all momentum, whereas Quadrants II and III are unstable.

The integrand is positive-definite ensuring convergence for a contour running along the real axis. Classically motivated, the NG modes should be fluctuations on top of a mean field homogeneous solution which should be asymptotically stable from the previous analysis. Taking functional variations of the action in gapped quantities and assuming that the mean field solutions are time-stationary and spatially homogeneous gives the first-order saddle-point equations. Functional differentiation with respect to $\rho_i(x,t)$ implies $\xi_i^{R/I} = 0$ for the quantum fields. Taking variations in the quantum fields $\xi_i^{R/I}$ gives the causal saddle-points for the dynamical equations of the retarded operator in the Keldysh action. Although non-trivial saddle-point solutions may exist, they are not considered here. In this approximation, the saddle-point equations become

$$\begin{aligned} \mu_c + \rho_1 u_c + \rho_2 v_c = 0,\ \mu_c + \rho_2 u_c + \rho_1 v_c = 0 \\ \mu_d - \rho_1 u_d - \rho_2 v_d = 0,\ \mu_d - \rho_2 u_d - \rho_1 v_d = 0 \end{aligned} \tag{S.24}$$

respecting the $\mathbb{Z}_2$ symmetry. This fixes the mean field density and provides a consistency relation determining the chemical potential μ_c. Expanding in fluctuations $\chi_i = \rho_i(x,t) - \rho$, ξ_i^R, ξ_i^I around the mean field $\phi_{i,0} = (\rho = \mu_d/(u_d + v_d), 0, 0)$, the action is expanded up to quadratic order in gapped fluctuations $\phi_i = (\rho_i, \xi_i^R, \xi_i^I)$ ignoring derivatives of gapped quantities (e.g. $\xi_i^R \partial_t \chi_i$ is set to zero). The expanded saddle-point action reads

$$S[\theta_i, \xi_i^R, \xi_i^I, \rho_i] = S_0[\phi_{i,0}, \theta_i] + \int_x \left.\frac{\delta S}{\delta \phi_i}\right|_0 (\phi_i - \phi_{i,0}) + \frac{1}{2}\int_x \left.\frac{\delta^2 S}{\delta\phi_i \delta\phi_j}\right|_0 (\phi_i - \phi_{i,0})(\phi_j - \phi_{j,0}) \,, \tag{S.25}$$

where the Hessian is a bilinear on field fluctuations. This saddle-point approximation breaks down in Quadrants II and III where the theory has unstable density modes. Key properties of the expanded action include: (i) $S_0[\phi_{i,0}]|_0 = 0$ due to vanishing quantum fields at the saddle-point, and (ii) static terms in $\delta S/\delta\phi_i|_0$ vanish, while derivatives in θ_i fields still contribute. This indicates that this is not a true saddle-point but more a classically motivated mean field solution. The contribution from the saddle-point term in the action reads:

$$\left.\frac{\delta S}{\delta \phi_i}\right|_0 (\phi_i - \phi_{i,0}) = \begin{pmatrix} \chi_1 \\ \chi_2 \\ \xi_1^R \\ \xi_2^R \\ \xi_1^I \\ \xi_2^I \end{pmatrix}^T \begin{pmatrix} 0 \\ 0 \\ -2\sqrt{\rho}(\partial_t \theta_1 + k_c(\partial_x\theta_1)^2 - k_d \partial_x^2\theta_1) \\ -2\sqrt{\rho}(\partial_t \theta_2 + k_c(\partial_x\theta_2)^2 - k_d \partial_x^2\theta_2) \\ 2\sqrt{\rho}(k_d(\partial_x\theta_1)^2 + k_c\partial_x^2\theta_1) \\ 2\sqrt{\rho}(k_d(\partial_x\theta_2)^2 + k_c\partial_x^2\theta_2) \end{pmatrix} \tag{S.26}$$

and contains couplings between derivatives of phase modes and quantum field fluctuations ξ_i. The Hessian introduces quadratic couplings in fluctuation fields, easily integrated out owing to their Gaussian structure. The Hessian contribution inherits a 6×6 structure in the gapped quantities and reads

$$\left.\frac{\delta^2 S}{\delta \phi_i \delta \phi_j}\right|_0 (\phi_i - \phi_{i,0})(\phi_j - \phi_{j,0}) = \begin{pmatrix} \chi_1 \\ \chi_2 \\ \xi_1^R \\ \xi_2^R \\ \xi_1^I \\ \xi_2^I \end{pmatrix}^T \begin{pmatrix} 0 & 0 & C_1 & M_1 & C_2 & M_2 \\ 0 & 0 & M_1 & C_1 & M_2 & C_2 \\ C_1 & M_1 & 2iN_1 & 2iN_2 & 0 & 0 \\ M_1 & C_1 & 2iN_2 & 2iN_1 & 0 & 0 \\ C_2 & M_2 & 0 & 0 & 2iN_1 & 2iN_2 \\ M_2 & C_2 & 0 & 0 & 2iN_2 & 2iN_1 \end{pmatrix} \begin{pmatrix} \chi_1 \\ \chi_2 \\ \xi_1^R \\ \xi_2^R \\ \xi_1^I \\ \xi_2^I \end{pmatrix}, \tag{S.27}$$

with a symmetric structure and parameters

$$C_1 = -\frac{3\rho u_c + \rho v_c + \mu_c}{2\sqrt{\rho}},\ C_2 = \frac{3\rho u_d + \rho v_d - \mu_d}{2\sqrt{\rho}},\ M_1 = -\sqrt{\rho}\, v_c,\ M_2 = \sqrt{\rho}\, v_d,\ N_1 = (2\rho u_d + \rho v_d + \gamma_T),\ N_2 = \rho v_d\,. \tag{S.28}$$

At this point, we highlight a key difference between starting with the SCGLE and mapping it to a stochastic path integral using MSRJD and the Hessian form shown in Eq. (S.27) directly from the path integral representation of the Lindbladian in the semiclassical limit. In the former, $N_2 = 0$ and the lower-right 4×4 block becomes diagonal as the noise is uncorrelated. The extension to allow χ integration limits between $[-\infty, \infty]$ is justified by noting that deviations from the mean field saddle-point contribute little to the integral. Expanding the Hessian out, we integrate out the χ_i modes:

$$\prod_i \int D[\chi_i] e^{i\int_x 2\sqrt{\rho}\chi_i\left(v_c(\xi_i^R - \xi_j^R) + u_d\xi_i^I + v_d\xi_j^I - \xi_i^R(u_c+v_c)\right)} = \prod_i \delta\left(u_d\xi_i^I + v_d\xi_j^I - v_c\xi_j^R - u_c\xi_i^R\right) \tag{S.29}$$

for $i \neq j$ and use the integral representation of the delta functional. The integral projects onto a manifold of trajectories where $\xi_i^{R/I}$ fluctuations are constrained by the delta functional conditions (S.29). The product of delta functions is non-trivial and demands discussion for carrying out the subsequent integral over ξ_i^I. We can consider a single point (x_0, t_0) noting that the argument of the delta function is time and spatially local and then generalise the argument for the entire integral. This involves integrating an expression like

$$\int_{U\subseteq\mathbb{R}^4} d\xi_1^I d\xi_2^I\ \delta(g(\xi_1^R, \xi_2^R, \xi_1^I, \xi_2^I))\ \delta(h(\xi_1^R, \xi_2^R, \xi_1^I, \xi_2^I)) f(\xi_1^R, \xi_2^R, \xi_1^I, \xi_2^I; \theta_1, \theta_2) \tag{S.30}$$

where g and h are the arguments of the delta functions from Eq. (S.29) and f is the remaining functional of gapped quantities and phase fields. After the constraints from the delta function, we have an integral over a surface given by $U \cap (g^{-1}(0) \cap h^{-1}(0))$. This is well-defined if g and h are linearly independent. Considering a diffeomorphism $\phi : V \to U$ such that $\xi \mapsto \phi(\xi) \in U$ allows for a change of variables,

$$\int_{U\subseteq\mathbb{R}^4} d\xi\ \delta(g(\xi))\ \delta(h(\xi)) f(\xi; \theta_1, \theta_2) \mapsto \int_{V\subseteq\mathbb{R}^4} d\xi \delta(g(\phi(x)))\delta(h(\phi(x))) f(\phi(x); \theta_1, \theta_2) J(\phi(\xi)), \tag{S.31}$$

to a coordinate system where the delta functions act on orthogonal spaces

$$\tilde{\xi}_1^I = u_d\xi_1^I + v_d\xi_2^I,\ \ \tilde{\xi}_2^I = v_d\xi_1^I + u_d\xi_2^I. \tag{S.32}$$

This is a valid diffeomorphism provided $u_d \neq v_d$ where the saddle-point approximation is unsuitable since a density instability arises. The delta functions now act on orthogonal spaces, allowing the integrals to be computed. In the original action in Eq. (S.8), intercomponent density-density interactions v_c, v_d mediate couplings of fields $\xi_i^{R/I}\chi_{\bar{i}}$ between the quantum and classical field fluctuations, while phase fluctuations θ_i only couple to quantum fields $\xi_i^{R/I}$ within the same component. Integrating out density fluctuation fields χ_i and ξ_i^I, gives rise to an effective cross-channel interaction between derivatives of the phase fluctuations and the real quantum fields. Computing the integrals, the low-energy effective theory is given by a multicomponent KPZ equation with full partition function reading

$$\mathcal{Z} = \int D[\boldsymbol{\theta}, \tilde{\boldsymbol{\xi}}^R] e^{i\int \left[\tilde{\xi}^R_\alpha \left(\partial_t \theta^\alpha - D^\alpha_\beta \partial_x^2 \theta^\alpha - \frac{1}{2}\Gamma^\alpha_{\beta\gamma}(\partial_x\theta^\beta)(\partial_x\theta^\gamma)\right) + i\ \tilde{\xi}_\alpha \Delta^\alpha_\beta \tilde{\xi}^\beta\right]} \tag{S.33}$$

with rescaled real quantum fields $\tilde{\xi}^R_\alpha = -2\sqrt{\rho}\,\xi_\alpha$. Owing to our semiclassical approximation, the form in Eq. (S.33) could be equivalently derived by starting in an Itô discretised multicomponent KPZ equation and mapping to a stochastic path integral using MSRJD. At this point, it is customary to introduce an auxiliary field using a Hubbard-Stratonovich transformation leading to the stochastic PDE Eq. (3) in Itô discretisation. The KPZ parameters in Eq. (S.33) are

$$\begin{gathered} D_{11} = k_c\mathcal{C}_1(u_d u_c - v_c v_d) + k_d,\ D_{12} = k_c\mathcal{C}_1(v_c u_d - u_c v_d), \\ \Gamma^1_{11} = -2k_c + 2k_d\mathcal{C}_1\left(u_c u_d - v_c v_d\right),\ \Gamma^1_{22} = 2k_d\mathcal{C}_1(v_c u_d - u_c v_d),\ \Gamma^1_{12} = 0 \end{gathered} \tag{S.34}$$

where $\mathcal{C}_1 = (u_d^2 - v_d^2)^{-1}$. The other coordinates can be inferred from the $\mathbb{Z}_2$ symmetry $1 \leftrightarrow 2$. All unspecified elements of the $\Gamma^\alpha_{\beta\gamma}$ tensor are zero. The covariance matrix has a complicated structure, however becomes diagonal in the normal mode basis

$$\tilde{\Delta}_{11} = \frac{\left((u_c+v_c)^2 + (u_d+v_d)^2\right)\left(2\rho(u_d+v_d)+\gamma_T\right)}{2\rho\left(u_d+v_d\right)^2},\ \tilde{\Delta}_{22} = \frac{\left((u_c-v_c)^2 + (u_d-v_d)^2\right)\left(2\rho u_d+\gamma_T\right)}{2\rho\left(u_d-v_d\right)^2}. \tag{S.35}$$

The non-rotated coordinates can be found by rotating

$$\Delta = \begin{pmatrix} \frac{1}{\sqrt{2}} & \frac{1}{\sqrt{2}} \\ \frac{1}{\sqrt{2}} & -\frac{1}{\sqrt{2}} \end{pmatrix} \cdot \begin{pmatrix} \tilde{\Delta}_{11} & \tilde{\Delta}_{12} \\ \tilde{\Delta}_{21} & \tilde{\Delta}_{22} \end{pmatrix} \cdot \begin{pmatrix} \frac{1}{\sqrt{2}} & \frac{1}{\sqrt{2}} \\ \frac{1}{\sqrt{2}} & -\frac{1}{\sqrt{2}} \end{pmatrix} \tag{S.36}$$

with $\tilde{\Delta}_{12} = \tilde{\Delta}_{21} = 0$. If we use the simpler form of the Action in Eq. (S.23) ignoring the additional cross-couplings as done in Eq. (S.10), the covariance matrix becomes

$$\tilde{\Delta}_{11} = \gamma_T \frac{\left((u_c+v_c)^2 + (u_d+v_d)^2\right)}{2\rho\left(u_d+v_d\right)^2},\ \tilde{\Delta}_{22} = \gamma_T \frac{\left((u_c-v_c)^2 + (u_d-v_d)^2\right)}{2\rho\left(u_d-v_d\right)^2} \tag{S.37}$$

and $\rho = \mu_d/(u_d+v_d)$ is the mean field density. In the limit $v_c, v_d \to 0$ the SCGLE become decoupled, agreeing with the form presented in Ref. [3]. The effective equations retain the $\mathbb{Z}_2$ degeneracy, motivating the symmetry constrained Wilsonian RG.

SUPPLEMENTARY NOTE 2 : PROPERTIES OF THE MULTICOMPONENT KPZ EQUATION

Before running the Wilsonian RG, we review concepts around the multicomponent KPZ equation to better interpret the flows. This section discusses the expected scaling form of the multicomponent KPZ solutions, the form of the adimensionalised equations useful for interpreting the RG flows, and the emergence of a stationary probability measure for the KPZ fields in specific submanifolds that satisfy the cyclicity condition for their interaction vertices in Eq. (3).

Scaling Form and Adimensionalisation

In the single-component case, KPZ solutions follow a scaling form

$$\theta(x,t) \sim t^{\chi/z} f(x/t^{1/z}) \tag{S.38}$$

where $\chi = 1/2$ is the roughness exponent, indicating that the theory is locally Brownian, and $z = 3/2$ defines the KPZ dynamical exponent. In Ref. [4], Prähofer and Spohn exactly determined the stationary KPZ distribution for the two-point correlation function. This scaling form implies that the transverse scale evolves as $t^{1/3}$ and the lateral scale evolves as $t^{2/3}$. For the single-component KPZ equation, we are at liberty to rescale the theory to have one characteristic parameter,

$$\partial_t\theta = \partial_x^2\theta + \sqrt{g}(\partial_x\theta)^2 + \sqrt{2}\zeta,\ \sqrt{g} = \frac{\lambda\epsilon^{1/2}\Delta^{1/2}}{2D^{3/2}}, \tag{S.39}$$

controlling the scaling behaviour: $g^* = 0$ is the Edwards-Wilkinson (EW) limit where $z = 2$, and $g^* = \pi/2$ is the KPZ fixed point in $d = 1$ predicted by Wilsonian RG. In Eq. (S.39), we have used a different protocol for the white noise with unit covariance, but switching to the covariance matrix definition used in the Eq. (3) is done by decomposing the coupled noise into two independent white noise processes. From the rotated KPZ Eq. (5), if $\tilde{D}^{\alpha\beta}$ is not proportional to $\mathbb{1}_{2\times2}$, we are unable to simply rescale our fields to have unit $\tilde{C}^{\alpha\beta} = [\tilde{D}^{-1}\tilde{\Delta}]^{\alpha\beta}$ for the rotated two-point correlation matrix of the non-interacting theory. When $\tilde{D}_{11} \neq \tilde{D}_{22}$, an additional scaling parameter emerges, requiring further investigation. To illustrate this, we derive the adimensionalised equations showcasing four relevant parameters. We construct a family of rescaled solutions indexed by ϵ for each field

$$\tilde{\theta}_1(x,t) = \epsilon^{\chi_1}\tilde{\theta}_1^\epsilon(\epsilon^{-1}x, \epsilon^{-z_1}t),\ \ \tilde{\theta}_2(x,t) = \epsilon^{\chi_2}\tilde{\theta}_2^\epsilon(\epsilon^{-1}x, \epsilon^{-z_2}t) \tag{S.40}$$

where we initially entertain the idea of independent scaling parameters z_1, z_2 in time, a condition which we will later abandon. This convention differs slightly with Ref. [5] with the microscopic to mesoscopic crossover corresponding to $\epsilon \to \infty$. In this scenario, the new derivatives are defined with respect to $x' = \epsilon^{-1}x$ and $t_1 = \epsilon^{-z_1}t$, $t_2 = \epsilon^{-z_2}t$. The dynamical equations in the rescaled fields become

$$\partial_{t_1}\tilde{\theta}_1^\epsilon = \epsilon^{z_1-2}\tilde{D}_{11}\partial_{x'}^2\tilde{\theta}_1^\epsilon + \frac{1}{2}\epsilon^{\chi_1+z_1-2}\tilde{\Gamma}^1_{11}(\partial_{x'}\tilde{\theta}_1^\epsilon)^2 + \frac{1}{2}\epsilon^{2\chi_2-\chi_1+z_1}\tilde{\Gamma}^1_{22}(\partial_{x'}\tilde{\theta}_2^\epsilon)^2 + \epsilon^{z_1-\chi_1}\frac{1}{\sqrt{\epsilon^{z_1+1}}}\sqrt{2\tilde{\Delta}_{11}}\zeta_1^\epsilon, \tag{S.41a}$$

$$\partial_{t_2}\tilde{\theta}_2^\epsilon = \epsilon^{z_2-2}\tilde{D}_{22}\partial_{x'}^2\tilde{\theta}_2^\epsilon + \epsilon^{\chi_1+z_2-2}\tilde{\Gamma}^2_{12}(\partial_{x'}\tilde{\theta}_1^\epsilon)(\partial_{x'}\tilde{\theta}_2^\epsilon) + \epsilon^{z_2-\chi_2}\frac{1}{\sqrt{\epsilon^{z_2+1}}}\sqrt{2\tilde{\Delta}_{22}}\zeta_2^\epsilon. \tag{S.41b}$$

where we have rescaled the noises appropriately. If we wish to set $\tilde{D}^{\alpha\beta} = \mathbb{1}_{2\times2}$, then we require that

$$\tilde{D}_{11}\cdot\epsilon^{z_1-2} = 1 \implies \epsilon^{z_1} = \epsilon^2/\tilde{D}_{11}, \tag{S.42a}$$

$$\tilde{D}_{22}\cdot\epsilon^{z_2-2} = 1 \implies \epsilon^{z_2} = \epsilon^2/\tilde{D}_{22}. \tag{S.42b}$$

This indicates that there is no way to rescale the theory to have a unit diffusion matrix without directly introducing an anisotropy in time scaling. Since the coupled SPDEs are defined with one consistent time unit, we continue with $z_1 = z_2$ and choose $\tilde{D}_{11}\epsilon^{z_1-2} = 1$. The noise terms can be rescaled by choosing

$$\epsilon^{z_1/2-\chi_1-1/2}\sqrt{\tilde{\Delta}_{11}} = 1 \implies \epsilon^{\chi_1} = \sqrt{\epsilon\tilde{\Delta}_{11}/\tilde{D}_{11}} \tag{S.43a}$$

$$\epsilon^{z_1/2-\chi_2-1/2}\sqrt{\tilde{\Delta}_{22}} = \sqrt{\tilde{D}_{22}/\tilde{D}_{11}} \implies \epsilon^{\chi_2} = \sqrt{\epsilon\tilde{\Delta}_{22}/\tilde{D}_{22}}. \tag{S.43b}$$

Here, the fields are scaled anisotropically. Using this, we define new parameters based on the rescaling:

$$\frac{1}{2}\tilde{\Gamma}^1_{11}\cdot\epsilon^{\chi_1+z_1-2} = \frac{\tilde{\Gamma}^1_{11}\epsilon^{1/2}\tilde{\Delta}_{11}^{1/2}}{2\tilde{D}_{11}^{3/2}} = \sqrt{Z} \tag{S.44a}$$

$$\frac{1}{2}\tilde{\Gamma}^1_{22}\cdot\epsilon^{2\chi_2-\chi_1+z_1-2} = \frac{\tilde{\Gamma}^1_{22}\tilde{\Delta}_{22}\epsilon^{1/2}}{2\tilde{D}_{22}\tilde{D}_{11}^{1/2}\tilde{\Delta}_{11}^{1/2}} = \frac{\tilde{\Delta}_{22}}{\tilde{\Delta}_{11}}\frac{\tilde{D}_{11}}{\tilde{D}_{22}}\frac{\tilde{\Gamma}^1_{22}}{\tilde{\Gamma}^1_{11}}\sqrt{Z} = Y\sqrt{Z}, \tag{S.44b}$$

$$\tilde{\Gamma}^2_{12}\cdot\epsilon^{\chi_1+z_1-2} = \frac{\tilde{\Gamma}^2_{12}\epsilon^{1/2}\tilde{\Delta}_{11}^{1/2}}{\tilde{D}_{11}^{3/2}} = 2\frac{\tilde{\Gamma}^2_{12}}{\tilde{\Gamma}^1_{11}}\sqrt{Z} = 2X\sqrt{Z}. \tag{S.44c}$$

and, upon defining $T = \tilde{D}_{22}/\tilde{D}_{11}$, we obtain the adimensionalised coupled KPZ equations

$$\begin{aligned}\partial_{t'}\tilde{\theta}_1^\epsilon &= \partial_{x'}^2\tilde{\theta}_1^\epsilon + \sqrt{Z}\left((\partial_{x'}\tilde{\theta}_1^\epsilon)^2 + Y(\partial_{x'}\tilde{\theta}_2^\epsilon)^2\right) + \sqrt{2}\zeta_1^\epsilon,\\ \partial_{t'}\tilde{\theta}_2^\epsilon &= T\partial_{x'}^2\tilde{\theta}_2^\epsilon + 2X\sqrt{Z}(\partial_{x'}\tilde{\theta}_1^\epsilon)(\partial_{x'}\tilde{\theta}_2^\epsilon) + \sqrt{2T}\zeta_2^\epsilon.\end{aligned} \tag{S.45}$$

This shows that, unlike in the single-component case where the RG analysis involves a single parameter g, the multicomponent KPZ equation requires analysis of an $\mathbb{R}^4$-space $\{T, X, Y, Z\}$ to fully classify the theory.

Hyperbolicity

In analysing Eq. (S.45), we assert that Quadrants II and IV in FIG. 2 are non-hyperbolic and exhibit an instability. This instability conflicts with the scaling form leading to non-KPZ features in the long-time and long-wavelength limit and can be shown at the dynamical level. Ignoring the white noise drive and mapping to the Burgers' equation for the velocity fields $\phi_1' = \partial_x \tilde{\theta}_1'$ and $\phi_2' = \partial_x \tilde{\theta}_2'$, we obtain

$$\partial_t \vec{\phi}' = \begin{pmatrix} \partial_x^2 & 0 \\ 0 & T\partial_x^2 \end{pmatrix} \vec{\phi}' + \sqrt{Z}\partial_x \left\{ \begin{pmatrix} \phi_1 & Y\phi_2 \\ X\phi_2 & X\phi_1 \end{pmatrix} \vec{\phi}' \right\}. \tag{S.46}$$

We seek a solution $\phi_1' = \epsilon_1 + \tilde{\phi}_1'(x,t)$ and $\phi_2' = \epsilon_2 + \tilde{\phi}_2'(x,t)$ where $(\epsilon_1, \epsilon_2) \in \mathbb{R}$, giving

$$\partial_t \vec{\tilde{\phi}}' = \sqrt{Z} \begin{pmatrix} 2\epsilon_1 & 2Y\epsilon_2 \\ 2X\epsilon_2 & 2X\epsilon_1 \end{pmatrix} \vec{\tilde{\phi}}' \tag{S.47}$$

where the Laplacian terms are sub-leading in the long-time behaviour. Stability imposes that the eigenvalues $\lambda_\pm = \sqrt{Z}\left((1+X)\epsilon_1 \pm \sqrt{(1-X)^2\epsilon_1^2 + 4XY\epsilon_2^2}\right)$ are real for all $(\epsilon_1,\, \epsilon_2)$ which is not guaranteed as the matrix is non-symmetric. In Quadrant I where $X,\, Y > 0$ and Quadrant III where $X,\, Y < 0$, the discriminant is always positive. In Quadrants II and IV this is not satisfied for all $(\epsilon_1,\, \epsilon_2)$ leading to non-hyperbolic behaviour and resulting in modes which grow exponentially in time.

Lyapunov and Stationary Measure

The KPZ equation can be framed as an infinite-dimensional analogue of an Itô discretised Langevin equation for a real-valued field. It is useful to understand the properties of the stationary measures, which can be motivated by considering an infinite-dimensional analogue to the Fokker-Planck equation. For fields, the probability density function gets elevated to a functional $\mathbb{P}[\{\tilde{\theta}(x,t)\};t]$ over the dynamical fields $\tilde{\theta}_i(x,t)$ at each point in space, obeying the generalisation of the Fokker-Planck equation

$$\partial_t \mathbb{P}[\tilde{\theta}] = -\int_x \delta_{\tilde{\theta}_x^\alpha} \left\{ \left[\tilde{D}_{\alpha\beta}\partial_x^2 \tilde{\theta}^\beta + \tilde{\Gamma}^\alpha_{\beta\gamma}(\partial_x \tilde{\theta}^\beta)(\partial_x \tilde{\theta}^\gamma) \right] \mathbb{P}[\{\tilde{\theta}\}] \right\} + \int_{x,y} \delta_{\tilde{\theta}_x^\alpha} \delta_{\tilde{\theta}_y^\alpha} \left[\tilde{\Delta}^{\alpha\beta}\delta(x-y)\mathbb{P}[\{\tilde{\theta}\}] \right]. \tag{S.48}$$

The derivative is a functional derivative $\delta_{\tilde{\theta}_x^\alpha} = \partial_{\tilde{\theta}_x^\alpha} - \partial_x \cdot \partial_{\partial_x \tilde{\theta}_x^\alpha}$. Ignoring the KPZ non-linearity, we seek a stationary probability measure $\partial_t \mathbb{P} = 0$ with the Gaussian ansatz

$$\mathbb{P}[\{\tilde{\theta}\}] = \int \mathcal{D}[\tilde{\theta}] \exp\left\{ -\frac{1}{2}\int_x (\partial_x \tilde{\theta}^\alpha) \tilde{C}^{-1}_{\alpha\beta} (\partial_x \tilde{\theta}^\beta) \right\} \tag{S.49}$$

where $\langle \partial_x \tilde{\theta}^\alpha \partial_y \tilde{\theta}^\beta \rangle = \tilde{C}^{\alpha\beta}\delta(x-y)$ is the symmetric same-time covariance matrix. Substituting the time stationary ansatz into Eq. (S.48) gives the Lyapunov condition $\mathbf{D} = \Delta C^{-1}$ which from symmetry gives $\mathbf{D}C + C\mathbf{D}^T = 2\Delta$ relating the two-point correlation function to the diffusion and noise matrices in the non-interacting theory. Defining rescaled interaction vertices $\hat{\Gamma}^\alpha = (\tilde{C}^{-1})_{\alpha\beta}\tilde{\Gamma}^\beta$, analogous to the adimensionalisation scheme, the non-interacting stationary measure remains time-stationary in the presence of interactions when the cyclicity condition $\hat{\Gamma}^\alpha_{\beta\gamma} = \hat{\Gamma}^\alpha_{\gamma\beta} = \hat{\Gamma}^\beta_{\gamma\alpha}$ is satisfied. The cyclicity condition for the two-component KPZ equation explicitly reads

$$\hat{\Gamma}^1 = \begin{pmatrix} a & b \\ b & c \end{pmatrix},\, \hat{\Gamma}^2 = \begin{pmatrix} b & c \\ c & d \end{pmatrix}. \tag{S.50}$$

Substituting the time-stationary measure from Eq. (S.49),

$$\int dx \left\{ \partial_x \left[-\frac{\tilde{\Gamma}^1_{11}\tilde{D}^{11}}{6\tilde{\Delta}_{11}} (\partial_x \tilde{\theta}_1)^3 \right] - \left[\frac{\tilde{\Gamma}^1_{22}\tilde{D}^{11}}{2\tilde{\Delta}_{11}} (\partial_x \tilde{\theta}_2)^2 \partial_x^2 \tilde{\theta}_1 + \frac{\tilde{\Gamma}^2_{12}\tilde{D}^{22}}{\tilde{\Delta}_{22}} (\partial_x \tilde{\theta}_1)(\partial_x \tilde{\theta}_2)\partial_x^2 \tilde{\theta}_2 \right] \right\} \mathbb{P}, \tag{S.51}$$

and requiring that the resulting integrand is at most a total derivative results in the stationary measure condition $\tilde{\Gamma}^1_{22}\tilde{D}_{11}\tilde{\Delta}_{22} = \tilde{\Gamma}^2_{12}\tilde{D}_{22}\tilde{\Delta}_{11}$. In this submanifold, the second term becomes a total derivative $\partial_x \left[(\partial_x \tilde{\theta}_2)^2 (\partial_x \tilde{\theta}_1) \right]$. This is equivalent to demanding $X = Y$ in adimensionalised coordinates. Additionally along this submanifold, the modes are described by same-time white noise processes with static scalings coinciding with the bare non-interacting theory $\chi_1 = \chi_2 = 1/2$. Importantly, the RG predicts that the long-wavelength theory is described by the emergence of a stationary measure in Quadrants I and III.

SUPPLEMENTARY NOTE 3 : WILSONIAN RENORMALISATION GROUP

In this section, we set up of the Wilsonian RG, starting from the MSRJD functional integral to give an equivalent action as in Eq. (S.33). The one-loop corrections are computed in the $\mathbb{Z}_2$-coordinates but the subsequent flows are interpreted in the adimensionalised coordinates in Eq. (S.45).

Martin-Siggia-Rose-Janssen-De Dominicis Functional

Motivated by Landau's symmetry arguments, we derive the general $\mathbb{Z}_2$-symmetric coupled KPZ equations, mapping to a field theory using the MSRJD formalism. The coupled equations are SPDEs driven by additive time-continuous centred Gaussian white noise processes $\{\zeta^\alpha(x,t)\}_{i=1}^2$ with symmetric covariance matrix $\Delta^{\alpha\beta} \in \mathbb{R}$ and $\Delta^{\alpha\beta} = \Delta^{\beta\alpha}$. The noises have multivariate probability density functional $W[\boldsymbol{\zeta}]$

$$W[\boldsymbol{\zeta}] \sim \exp\left\{-\frac{1}{4}\int_{x,t} \zeta^\alpha \Delta^{-1}_{\alpha\beta}\zeta^\beta\right\} \tag{S.52}$$

preserving normalisation $\int \mathcal{D}[\boldsymbol{\zeta}]W[\boldsymbol{\zeta}] = 1$. Changing variables $\{\boldsymbol{\zeta}(x,t)\} \mapsto \{\boldsymbol{\theta}(x,t)\}$ gives the Onsager-Machlup functional for the dynamical field probability distribution

$$\mathcal{P}[\boldsymbol{\theta}(x,t)] \sim \left|\det\left\{\frac{\mathcal{D}\boldsymbol{\theta}(x,t)}{\mathcal{D}\boldsymbol{\zeta}(\boldsymbol{x}',t')}\right\}\right| \exp\left\{-\frac{1}{4}\int_{x,t} \left(\partial_t\theta^\alpha - F^\alpha[\boldsymbol{\theta}]\right)\Delta^{-1}_{\alpha\beta}\left(\partial_t\theta^\beta - F^\beta[\boldsymbol{\theta}]\right)\right\}. \tag{S.53}$$

Although we have taken liberty to pose the solutions to the stochastic PDE in the language of continuous functions, the solutions are almost nowhere-differentiable. Even for stochastic ODEs, non-differentiability requires a discretisation scheme to properly interpret integration. This problem pervades to the level of the path integral in the Jacobian prefactor. However, the Itô discretisation simplifies matters, as the Jacobian becomes independent of the dynamical field $\boldsymbol{\theta}(\boldsymbol{x},t)$ and can be dropped. Introducing a purely imaginary response field $\chi_i : \mathbb{R}^d \times \mathbb{R} \to i\mathbb{R}$ with a Hubbard-Stratonovich transformation gives Action (S.33). In Fourier space, using the convention in Eq. (S.13) with $k = (\omega, \vec{k})$, the action becomes

$$\begin{aligned} S[\theta_1,\theta_2,\chi_1,\chi_2] = \Bigg[\int_{k_1} &\Big[\chi_{1,k_1}\left(-i\omega\,\eta\,\theta_{1,-k_1} + D_{11}k_1^2\theta_{1,-k_1} + D_{12}k_1^2\theta_{2,-k_1}\right) - \chi_{1,k_1}\Delta_{11}\chi_{1,-k_1} - \chi_{1,k_1}\Delta_{12}\chi_{2,-k_1}\Big] \\ &+ \int_{k_1,k_2,k_3} k_2\cdot k_3\left[\chi_{1,k_1}\left(\frac{\Gamma^1_{11}}{2}\theta_{1,k_2}\theta_{1,k_3} + \Gamma^1_{12}\theta_{1,k_2}\theta_{2,k_3} + \frac{\Gamma^1_{22}}{2}\theta_{2,k_2}\theta_{2,k_3}\right)\delta_{k_1,k_2,k_3}\right]\Bigg] + (1 \leftrightarrow 2) \end{aligned} \tag{S.54}$$

where subscripts indicate field component and momentum. The parameter η scales the time derivative, but receives no RG corrections. The first line of Eq. (S.54) describes the Gaussian theory, providing the bare propagators, while the second line contains the 3-point KPZ interaction vertices with frequency and momentum conserving delta functions.

Non-Interacting Theory

It is insightful to represent the Gaussian theory in Eq. (S.54) in a higher dimensional space to derive propagator rules. Integrating by parts and symmetrising, the inverse propagator matrix reads

$$\hat{\mathbf{G}}^{-1}_{0,k_1} = \begin{pmatrix} -2\Delta_{11} & i\eta\omega + D_{11}k^2 & -2\Delta_{12} & D_{12}k^2 \\ -i\eta\omega + D_{11}k^2 & 0 & D_{12}k^2 & -2\Delta_{12} \\ -2\Delta_{12} & D_{12}k^2 & -2\Delta_{11} & i\eta\omega + D_{11}k^2 \\ D_{12}k^2 & -2\Delta_{12} & -i\eta\omega + D_{11}k^2 & 0 \end{pmatrix} \tag{S.55}$$

for the vectorised space $\Psi = (\chi_1, \theta_1, \chi_2, \theta_2)$ in the Fourier representation. Taking functional derivatives of the generating function $\mathcal{Z}[\boldsymbol{J}]$, the bare two-point correlators are

$$G_0(k,\omega) = \langle \theta_{\alpha,k}\chi_{\alpha,-k}\rangle = \frac{-D_{11}k^2 + i\omega}{(\omega + i(D_{11}+D_{12})k^2)(\omega + i(D_{11}-D_{12})k^2)} \tag{S.56a}$$

$$C_o(k,\omega) = \langle \theta_{\alpha,k}\theta_{\alpha,-k}\rangle = \frac{2\Delta_{11}(\omega^2 + (D_{11}^2 + D_{12}^2)k^4) - 4\Delta_{12}D_{11}D_{12}k^4}{(\omega - i(D_{11}+D_{12})k^2)(\omega - i(D_{11}-D_{12})k^2)(\omega + i(D_{11}+D_{12})k^2)(\omega + i(D_{11}-D_{12})k^2)} \tag{S.56b}$$

$$T_0(k,\omega) \underset{\alpha\neq\beta}{=} \langle \theta_{\alpha,k}\chi_{\beta,-k}\rangle = \frac{D_{12}k^2}{(\omega + i(D_{11}+D_{12})k^2)(\omega + i(D_{11}-D_{12})k^2)} \tag{S.56c}$$

$$Q_0(k,\omega) \underset{\alpha\neq\beta}{=} \langle \theta_{\alpha,k}\theta_{\beta,-k}\rangle = \frac{2\Delta_{12}(\omega^2 + (D_{11}^2 + D_{12}^2)k^4) - 4\Delta_{11}D_{11}D_{12}k^4}{(\omega - i(D_{11}+D_{12})k^2)((\omega - i(D_{11}-D_{12})k^2)(\omega + i(D_{11}+D_{12})k^2)(\omega + i(D_{11}-D_{12})k^2)}. \tag{S.56d}$$

In total, there are 16 possible propagators, which reduce to 8 due to the $\mathbb{Z}_2$ symmetry. The off-diagonal terms are related by inversion in frequency space $\omega \mapsto -\omega$, from time-ordering and causality, leaving four propagators: G_0, C_0, T_0, Q_0. Closed response loops vanish in the Itô discretisation $\langle \chi_{\alpha,k_1}\chi_{\beta,-k_1}\rangle = 0$ from causality. The response-phase connected correlation functions have poles lying in the lower-half plane, maintaining causality.

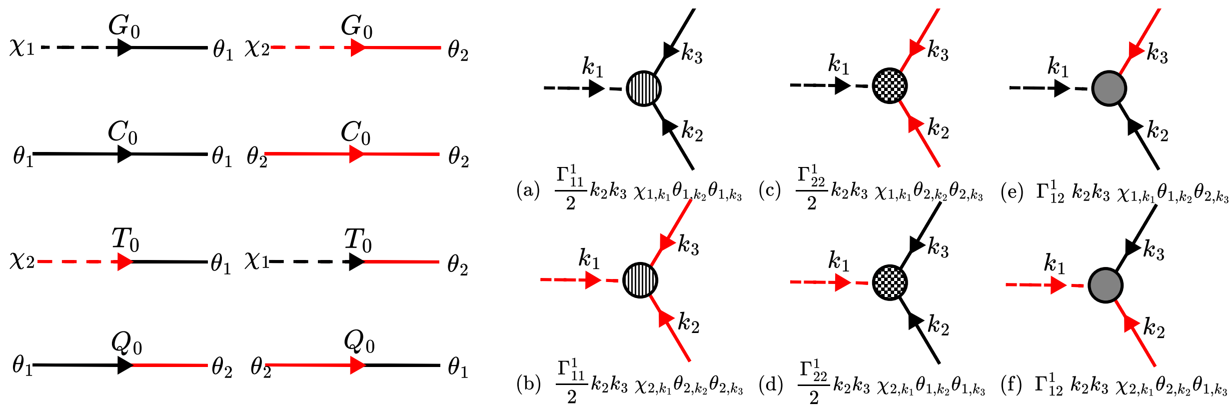

(S.57)

Pictorially, response fields are represented by dashed lines with red or black edges distinguishing $(1,2)$ fields respectively. Phase fields are denoted by solid lines. Arrows signify the response field $\chi_{\alpha,-k}$ *transmutating* into a dynamical field $\theta_{\alpha,k}$, corresponding to closing the contour in the lower-half plane for causality. Although there are 24 potential interaction vertices, symmetry constraints reduce this to six, with three coupling constants Γ^1_{11}, Γ^1_{12}, Γ^1_{22}.

Wilsonian Renormalisation Group

Wilsonian RG generates scale-dependent theories by elevating the parameters to functions of the RG scale ℓ, capturing the long-wavelength physics as $\ell \to \infty$. This can be done by iteratively integrating out fast fluctuations. The momentum is split between slow fields $0 \leq k < \Lambda/b$ and fast fields $\Lambda/b \leq k \leq \Lambda$, where Λ is the momentum cut-off regularising the theory in the UV and b is a real parameter. From linearity, $\theta_i = \theta_i^s(\omega,k) + \theta_i^f(\omega,k)$. The integral measures for fast and slow fields decouple, allowing us to define a theory over the slow modes with a statistical weight factor after integrating out the fast fields

$$\mathbb{W}[\boldsymbol{\theta}^s,\boldsymbol{\chi}^s] = \int D[\boldsymbol{\theta}^f,\boldsymbol{\chi}^f]\exp\left\{\underbrace{-A_0[\boldsymbol{\theta}^s,\boldsymbol{\chi}^s]}_{\text{S Gaussian}} - \underbrace{A_I[\boldsymbol{\theta}^s,\boldsymbol{\chi}^s]}_{\text{S Int}} - \underbrace{A_0[\boldsymbol{\theta}^f,\boldsymbol{\chi}^f]}_{\text{F Gaussian}} - \underbrace{A_I[\boldsymbol{\theta}^f,\boldsymbol{\chi}^f]}_{\text{F Int}} - \underbrace{\tilde{A}_I[\boldsymbol{\theta}^s,\boldsymbol{\chi}^s,\boldsymbol{\theta}^f,\boldsymbol{\chi}^f]}_{\text{S−F Int}}\right\} \tag{S.58}$$

where $A_0[\boldsymbol{\theta}^f,\boldsymbol{\chi}^f]$ is the Gaussian statistical weight for fast fields. This involves computing the expectation value $\langle \exp[-\tilde{A}_I[\boldsymbol{\theta}^s,\boldsymbol{\chi}^s,\boldsymbol{\theta}^f,\boldsymbol{\chi}^f]]\rangle$ with respect to the probability measure over fast fields. The fast field probability distribution is typically assumed to be Gaussian, as including interaction terms leads to higher-order corrections than 1-loop. Thus the effective statistical weight for the slow fields becomes:

$$\mathbb{W}[\boldsymbol{\theta}^s,\boldsymbol{\chi}^s] = e^{-A[\boldsymbol{\theta}^s,\boldsymbol{\chi}^s]}\langle e^{-\tilde{A}_I[\boldsymbol{\theta}^s,\boldsymbol{\chi}^s,\boldsymbol{\theta}^f,\boldsymbol{\chi}^f]}\rangle_f \tag{S.59}$$

where $\langle\cdot\rangle_f$ indicates integration over fast fields using Wick's theorem such that all cumulants vanish for $n > 2$. The Wilsonian Effective Action is defined as:

$$A'[\boldsymbol{\theta}^s,\boldsymbol{\chi}^s] = A[\boldsymbol{\theta}^s,\boldsymbol{\chi}^s] - \log\langle e^{-\tilde{A}_I[\boldsymbol{\theta}^s,\boldsymbol{\chi}^s,\boldsymbol{\theta}^f,\boldsymbol{\chi}^f]}\rangle_f\,, \tag{S.60}$$

and generates the connected subset of all possible graphs. To calculate the renormalised parameters, we use a perturbative expansion in interactions around the Gaussian fixed point. Expanding the logarithm yields the corrections:

$$\text{Corrections} = \langle \tilde{A}_I \rangle_c - \frac{1}{2!}\langle \tilde{A}_I^2 \rangle_c + \frac{1}{3!}\langle \tilde{A}_I^3 \rangle_c. \tag{S.61}$$

Calculating the renormalised terms to 1-loop requires automation of generating connected diagrams. An Important point to highlight is that integration over χ_i^f is over the imaginary axis from $(-i\infty, i\infty)$ yielding an additional minus sign from Wick rotation. In the 1-loop corrections, we assume analyticity of the resulting integrals in slow momenta k_s and frequency ω_s. The corrections involve integrals of the form:

$$\begin{aligned} \int_{\omega,k} f(\omega, k, \omega_s, k_s) &= \int_{\omega,k} \sum_{n,m=0} \omega_s^n k_s^m f^{(n,m)}(\omega, k) \\ &\stackrel{!}{=} \sum_{n,m=0} \omega_s^n k_s^m \int_{\omega,k} f^{(n,m)}(\omega, k) \end{aligned} \tag{S.62}$$

where f is a product of propagators and interaction vertices. (k, ω) are the free-momentum around the loop and (k_s, ω_s) are the incoming momentum. If the order of the infinite sum and integral can be exchanged, the relevant corrections can be found in the series expansion in slow variables. In the spirit of non-covariant theories, there is no cutoff in frequency, and the resulting frequency integral runs over the real line. The domain of integration for the momentum in Cartesian coordinates is given by the set of points for which $\mathcal{D} = \{(x_1, x_2, \ldots) | \Lambda/b \leq \sqrt{\sum x_i^2} \leq \Lambda\}$ defining a shell in momentum space for the fast modes. Two frequently appearing integrals are:

$$\int_{\mathcal{D}} \frac{d^d q}{(2\pi)^d} \frac{1}{q^2} = \frac{1}{2^{d-1}\Gamma(d/2)\pi^{d/2}} \Lambda^{d-2}\, d\ell = K_d\, d\ell \tag{S.63}$$

which diverges in the infrared as $q \to 0$ for $d_c \leq 2$. This divergence does not appear in our integrals over a slice, and

$$\int_{\mathcal{D}} \frac{d^d q}{(2\pi)^d} \frac{(k_s \cdot q)^2}{(q^4)} = k_s^i k_s^j \int_{\mathcal{D}} \frac{d^d q}{(2\pi)^d} \frac{q^i q^j}{(q^4)} != k_s^i k_s^j \frac{\delta_{ij}}{d} \int_{\mathcal{D}} \frac{d^d q}{(2\pi)^d} \frac{1}{q^2} = \frac{k_s \cdot k_s}{d} K_d\, d\ell. \tag{S.64}$$

which appeals to Passerino-Veltman arguments. At this stage, we calculate the corrections from Eq. (S.61) for the parameters in the $\mathbb{R}^8$-parameter space $\mathcal{P} = \{\eta, D_{11}, D_{12}, \Gamma^1_{11}, \Gamma^1_{12}, \Gamma^1_{22}, \Delta_{11}, \Delta_{12}\}$. No corrections are generated for η which would require terms $\omega_s \chi_s^\alpha \theta_s^\alpha$ in the Wilsonian effective action. The non-covariant theory exhibits anisotropic scaling in space and time

$$x \mapsto bx\ ,\ t \mapsto b^z t\ ,\ \theta^\alpha \mapsto b^\chi \theta^\alpha\ ,\ \chi^\alpha \mapsto b^{\tilde{\xi}} \chi^\alpha \tag{S.65}$$

as well as scaling to the response fields. We assume a single time-scaling parameter, which is valid in the non-decoupled case of Eq. (S.45) within the normal mode space. However, $X = 0$ is an exceptional point allowing independent time rescaling for both modes. This is equivalent to demanding that in the RG limit, there is one scaling parameter and the resulting two-point functions take on the scaling form

$$\langle \theta_\alpha \theta_\beta \rangle \sim t^{\chi/z} C_{\alpha\beta}(x/t^{1/z}) \tag{S.66}$$

where χ and z are to be determined. The $\mathbb{Z}_2$ symmetry is preserved under RG. The corrections for each parameter are calculated, and comparisons are drawn to the single-component case.

Corrections to Covariance Matrix

The one-loop corrections to the covariance matrix $\Delta_{\alpha\beta}$ arise from terms in the expansion of the Wilsonian effective action (S.60) proportional to $\chi^s_\alpha \chi^s_\beta$, specifically in $-(1/2)\langle \tilde{A}_I^2 \rangle_c$. For instance, corrections for Δ_{11} can be represented by diagrammatic sums

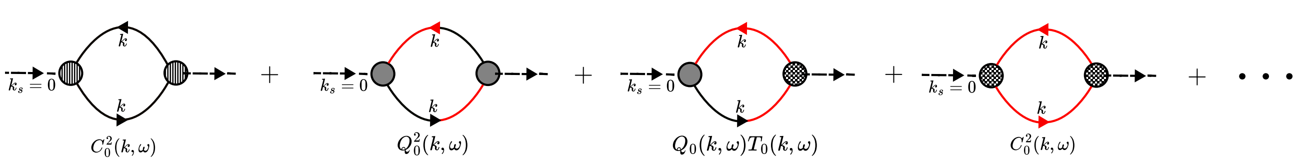

(S.67)

where χ_1^s are outgoing-legs. The internal propagators are products of phase-phase correlators, either Q_0 or C_0. The degeneracy of each diagram is calculated via automated combinatorics by directly expanding the action. The corrections to Δ_{11} are simplified by setting in-going momentum to zero from argument Eq. (S.62). The loop corrections, $\text{-}\bigcirc\text{-}$, for Δ_{11} and Δ_{12} are:

$$\begin{aligned}
[\text{-}\bigcirc\text{-}]_{\Delta_{11}} &= -\frac{1}{4}\int \frac{d^dk}{(2\pi)^d}\frac{d\omega}{2\pi}(k\cdot k)^2\left[((\Gamma^1_{11})^2+2(\Gamma^1_{12})^2+(\Gamma^1_{22})^2)C_0^2+4\Gamma^1_{12}(\Gamma^1_{11}+\Gamma^1_{22})C_0Q_0+2((\Gamma^1_{12})^2+\Gamma^1_{11}\Gamma^1_{22})Q_0^2\right]\\
[\text{-}\bigcirc\text{-}]_{\Delta_{12}} &= -\frac{1}{4}\int \frac{d^dk}{(2\pi)^d}\frac{d\omega}{2\pi}(k\cdot k)^2\left[((\Gamma^1_{11})^2+2(\Gamma^1_{12})^2+(\Gamma^1_{22})^2)Q_0^2+4\Gamma^1_{12}(\Gamma^1_{11}+\Gamma^1_{22})C_0Q_0+2((\Gamma^1_{12})^2+\Gamma^1_{11}\Gamma^1_{22})C_0^2\right]
\end{aligned} \tag{S.68}$$

where the 1/4 prefactor comes from symmetrising the corrections $\Delta_{12}=\Delta_{21}$ and the minus comes from the expansion. By $\mathbb{Z}_2$ symmetry, Δ_{11}=Δ_{22} and the flow equation can be deduced directly. The integrals over frequency are calculated by closing the integral in the lower complex plane and using Jordan's Lemma and Cauchy Residue Theorem. The covariance matrix corrections are

$$-\int_{x,t}\left[\Delta_{\alpha\beta}b^{z+2\tilde{\xi}+d}-\text{-}\bigcirc\text{-}\right]\chi_\alpha\chi_\beta \implies \partial_\ell\Delta_{\alpha\beta}=\left(z+2\tilde{\xi}+d-\frac{[\text{-}\bigcirc\text{-}]_{\Delta_{\alpha\beta}}}{\Delta_{\alpha\beta}}\right)\Delta_{\alpha\beta} \tag{S.69}$$

from which the infinitesimal RG equations are calculated. They become more instructive in the normal mode basis where:

$$[\text{-}\bigcirc\text{-}]_{\tilde{\Delta}_{11}}=-\frac{K_d\left((\tilde{\Gamma}^1_{11})^2\tilde{\Delta}^2_{11}\tilde{D}^3_{22}+\tilde{D}^3_{11}(\tilde{\Gamma}^1_{22})^2\tilde{\Delta}^2_{22}\right)}{4\tilde{D}^3_{11}\tilde{D}^3_{22}},\ [\text{-}\bigcirc\text{-}]_{\tilde{\Delta}_{22}}=-\frac{K_d\left((\tilde{\Gamma}^2_{12})^2\tilde{\Delta}_{11}\tilde{\Delta}_{22}\right)}{\tilde{D}_{11}\tilde{D}_{22}(\tilde{D}_{11}+\tilde{D}_{22})}. \tag{S.70}$$

As a consistency check, the corrections to $\tilde{\Delta}_{11}$ agree with the single-component KPZ RG corrections from $\tilde{\Gamma}_{11}$, but with an additional contribution from $\tilde{\Gamma}^1_{22}$ with the same structure but different propagators.

Corrections to Diffusion Matrix

For the 1-loop corrections to the diffusive matrix elements D_{11} and D_{12}, we introduce non-zero incoming and outgoing momenta, labelled as k_s to generate terms of the form $k_s^2\chi^s_\alpha\theta^s_\beta$. The corrections to D_{11} are

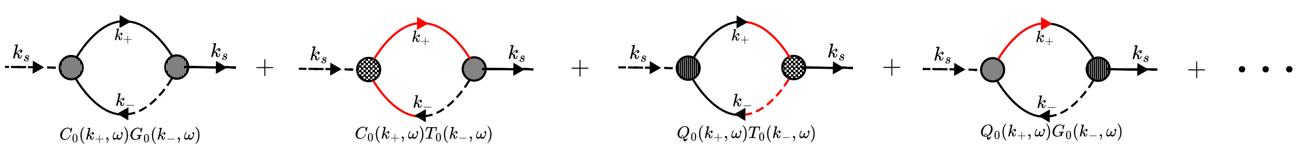

(S.71)

where k_s is the incoming momentum and $k_\pm=k\pm\frac{k_s}{2}$. Since there is no outgoing slow frequency dependence, $\omega_s=0$ ensuring the frequency in the internal loop is the same. The momentum dependence also appears in the vertex factors. All diagrams in Eq. (S.71) have the same topology with momentum contribution factor

$$f(k,k_s)=[k+k_s/2]\cdot[k-k_s/2]\,[k+k_s/2]\cdot[-k_s] \tag{S.72}$$

where the interaction vertex has convention that the momentums are incoming. Focusing on terms proportional to $k_s\cdot k_s$, the total correction $\text{-}\bigcirc\text{-}$ is given by:

$$\begin{aligned}
[\text{-}\bigcirc\text{-}]_{D_{11}}=-\int\frac{d^dk}{(2\pi)^d}\frac{d\omega}{2\pi}f(k,k_s)\Big[&((\Gamma^1_{11})^2+(\Gamma^1_{12})^2+2\Gamma^1_{12}\Gamma^1_{22})C_{0,k_+}G_{0,k_-}+((\Gamma^1_{12})^2+2\Gamma^1_{11}\Gamma^1_{12}+(\Gamma^1_{22})^2)Q_{0,k_+}G_{0,k_-}\\
&+(\Gamma^1_{11}+\Gamma^1_{12})(\Gamma^1_{22}+\Gamma^1_{12})\left(C_{0,k_+}T_{0,k_-}+Q_{0,k_+}T_{0,k_-}\right)\Big]
\end{aligned} \tag{S.73}$$

and for the off-diagonal term D_{12}

$$\begin{aligned}
[\text{-}\bigcirc\text{-}]_{D_{12}}=-\int\frac{d^dk}{(2\pi)^d}\frac{d\omega}{2\pi}f(k,k_s)\Big[&((\Gamma^1_{11})^2+(\Gamma^1_{12})^2+2\Gamma^1_{12}\Gamma^1_{22})Q_{0,k_+}T_{0,k_-}+((\Gamma^1_{12})^2+2\Gamma^1_{11}\Gamma^1_{12}+(\Gamma^1_{22})^2)C_{0,k_+}T_{0,k_-}\\
&+(\Gamma^1_{11}+\Gamma^1_{12})(\Gamma^1_{22}+\Gamma^1_{12})\left(Q_{0,k_+}G_{0,k_-}+C_{0,k_+}G_{0,k_-}\right)\Big].
\end{aligned} \tag{S.74}$$

We first integrate over ω to zeroth order in ω_s, then expand the integrand to $O(k_s^2)$. The action receives correction

$$-\int_{\omega,k}\left[D_{\alpha\beta}b^{z+\chi+\tilde{\xi}+d-2}+\;\right]\chi_\alpha\partial_x^2\theta_\beta \implies \partial_\ell D_{\alpha\beta}=\left(z+\chi+\tilde{\xi}+d-2+\frac{[\;]_{D_{\alpha\beta}}}{D_{\alpha\beta}}\right)D_{\alpha\beta} \tag{S.75}$$

where the additional minus comes from going back to the real space representation of the fields $q_s^2 \mapsto -\partial_x^2$. The corrections in the rotated basis become:

$$\begin{aligned}
[\;]_{\tilde{D}_{11}} &= \frac{(2-d)\left(\tilde{D}_{22}^2\tilde{\Delta}_{11}(\tilde{\Gamma}_{11}^1)^2+\tilde{D}_{11}^2\tilde{\Delta}_{22}\tilde{\Gamma}_{22}^1\tilde{\Gamma}_{12}^2\right)}{4d\tilde{D_{11}}^2\tilde{D_{22}}^2}K_d\\
[\;]_{\tilde{D}_{22}} &= \left(\tilde{\Gamma}_{22}^1\tilde{\Gamma}_{12}^2\tilde{\Delta}_{22}M_{\tilde{D}_{11},\tilde{D}_{22}}+(\tilde{\Gamma}_{12}^2)^2\tilde{\Delta}_{11}M_{\tilde{D}_{22},\tilde{D}_{11}}\right)K_d\\
M_{\tilde{D}_{11},\tilde{D}_{22}} &= \frac{\left((4-d)\tilde{D}_{22}-d\tilde{D}_{11}\right)}{2d\tilde{D}_{22}\left(\tilde{D}_{11}+\tilde{D}_{22}\right)^2}.
\end{aligned} \tag{S.76}$$

For $\tilde{D}_{11}$, there is the standard KPZ correction from the single-component and an additional cross-component with the same structure. In agreement with the single-component KPZ equation, the corrections to $\tilde{D}_{11}$ vanish at $d_c = 2$. The term $\tilde{D}_{22}$ is renormalised only by the cross-component interaction, resulting in a different structure.

Corrections to Non-linear Terms

In the single-component case, the non-linear term does not receive corrections due to the infinitesimal Galilean invariance of the MSR action, which leads to Ward-Takahashi Identities relating the RG flow of η to the non-linearity Γ [6]. In the coupled $\mathbb{Z}_2$ theory, this symmetry is lost and all $\Gamma_{\beta\gamma}^\alpha$ receive corrections. There are three distinct diagrammatic topologies based on momentum flow: (a1-a2) asymmetric graphs and (s1) symmetric graphs. Depending on the momentum flow and the direction of the retarded Green's functions, each topology has a different number of poles in the lower half-plane. To illustrate this, we examine the intracomponent contributions to Γ_{11}^1, where no propagators contain fields indexed by 2, as shown below:

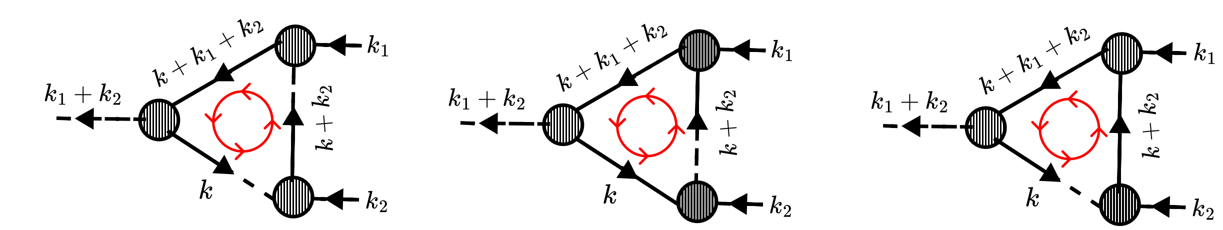

$G_0(-k)G_0(-k-k_2)C_0(k+k_1+k_2)$ (a1) $\quad$ $G_0(k+k_1+k_2)G_0(k+k_2)C_0(k)$ (a2) $\quad$ $G_0(k+k_1+k_2)G_0(-k)C_0(k+k_2)$ (s1). (S.77)

In these diagrams, k_1 and k_2 are the incoming momenta of the phase fields and the red loop indicates the internal momentum flow. Corrections from the asymmetric terms (a1-a2) are equal but differ in the number of poles in the lower half-plane: (a1) has two poles, (a2) has six poles, and (s1) has four poles. Moreover, the momentum dependent vertex factors are different between topologies. We include the full expressions for the corrections which are long and sadly not that enlightening. The symmetric contributions (s1) are:

$$
\begin{aligned}
\left[-\!\!\bigcirc\!\!-\right]^{\mathrm{s1}}_{\Gamma^1_{11}} &= -\int \frac{d^dk}{(2\pi)^d}\frac{d\omega}{2\pi} f_{(\mathrm{s1})}(k,k_1,k_2)\Big[M_1\left(G_{0,-k}G_{0,q}C_{0,r}\right) + M_2\left(T_{0,-k}G_{0,q}C_{0,r} + G_{0,-k}T_{0,q}C_{0,r}\right) \\
&+ M_3\left(T_{0,-k}T_{0,q}C_{0,r}\right) + M_4\left(G_{0,-k}G_{0,q}Q_{0,r}\right) + M_5\left(T_{0,-k}G_{0,q}Q_{0,r} + G_{0,-k}T_{0,q}Q_{0,r}\right) + M_6\left(T_{0,-k}T_{0,q}Q_{0,r}\right)\Big], \\
\left[-\!\!\bigcirc\!\!-\right]^{\mathrm{s1}}_{\Gamma^1_{12}} &= -\int \frac{d^dk}{(2\pi)^d}\frac{d\omega}{2\pi} f_{(\mathrm{s1})}(k,k_1,k_2)\Big[M_5\left(G_{0,-k}G_{0,q}C_{0,r}\right) + M_4\left(T_{0,-k}G_{0,q}C_{0,r}\right) + M_6\left(G_{0,-k}T_{0,q}C_{0,r}\right) \\
&+ M_5\left(T_{0,-k}T_{0,q}C_{0,r}\right) + M_2\left(G_{0,-k}G_{0,q}Q_{0,r}\right) + M_1\left(T_{0,-k}G_{0,q}Q_{0,r}\right) + M_3\left(G_{0,-k}T_{0,q}Q_{0,r}\right) + M_2\left(T_{0,-k}T_{0,q}Q_{0,r}\right)\Big], \\
\left[-\!\!\bigcirc\!\!-\right]^{\mathrm{s1}}_{\Gamma^1_{22}} &= -\int \frac{d^dk}{(2\pi)^d}\frac{d\omega}{2\pi} f_{(\mathrm{s1})}(k,k_1,k_2)\Big[M_3\left(G_{0,-k}G_{0,q}C_{0,r}\right) + M_2\left(T_{0,-k}G_{0,q}C_{0,r} + G_{0,-k}T_{0,q}C_{0,r}\right) \\
&+ M_1\left(T_{0,-k}T_{0,q}C_{0,r}\right) + M_6\left(G_{0,-k}G_{0,q}Q_{0,r}\right) + M_5\left(T_{0,-k}G_{0,q}Q_{0,r} + G_{0,-k}T_{0,q}Q_{0,r}\right) + M_4\left(T_{0,-k}T_{0,q}Q_{0,r}\right)\Big],
\end{aligned}
\tag{S.78}
$$

where $q = k + k_1 + k_2$ and $r = k + k_2$ and M_i are constants that are polynomials of interaction vertices

$$
\begin{aligned}
M_1 &= -\frac{1}{2}\left((\Gamma^1_{11})^3 + \Gamma^1_{12}\left(\Gamma^1_{12} + 2\Gamma^1_{22}\right)\Gamma^1_{11} + 2(\Gamma^1_{12})^3 + (\Gamma^1_{22})^3 - (\Gamma^1_{12})^2\Gamma^1_{22}\right) \\
M_2 &= -\frac{1}{2}\left(\left(\left(\Gamma^1_{12} + \Gamma^1_{22}\right)(\Gamma^1_{11})^2\right) + \left((\Gamma^1_{12})^2 + (\Gamma^1_{22})^2\right)\Gamma^1_{11} + \Gamma^1_{12}\left(2(\Gamma^1_{12})^2 + \Gamma^1_{22}\Gamma^1_{12} + (\Gamma^1_{22})^2\right)\right) \\
M_3 &= -\frac{1}{2}\left(\Gamma^1_{11} + 2\Gamma^1_{12} + \Gamma^1_{22}\right)\left((\Gamma^1_{12})^2 + \Gamma^1_{11}\Gamma^1_{22}\right) \\
M_4 &= -\Gamma^1_{12}\left((\Gamma^1_{11})^2 + \Gamma^1_{12}\Gamma^1_{11} + \Gamma^1_{22}\left(\Gamma^1_{12} + \Gamma^1_{22}\right)\right) \\
M_5 &= -\frac{1}{2}\Gamma^1_{12}\left(\Gamma^1_{11} + \Gamma^1_{22}\right)\left(\Gamma^1_{11} + 2\Gamma^1_{12} + \Gamma^1_{22}\right) \\
M_6 &= -\Gamma^1_{12}\left(\Gamma^1_{12}\Gamma^1_{22} + \Gamma^1_{11}\left(\Gamma^1_{12} + 2\Gamma^1_{22}\right)\right).
\end{aligned}
\tag{S.79}
$$

The asymmetric terms (a1-a2) are equal. The corrections to the (a1) topologies are:

$$
\begin{aligned}
\left[-\!\!\bigcirc\!\!-\right]^{\mathrm{a1}}_{\Gamma^1_{11}} &= -\int \frac{d^dk}{(2\pi)^d}\frac{d\omega}{2\pi} f_{(\mathrm{a1})}(k,k_1,k_2)\Big[\tilde{M}_1\left(G_{0,-k}G_{0,-r}C_{0,q}\right) + \tilde{M}_2\left(T_{0,-k}G_{0,-r}C_{0,q}\right) + \tilde{M}_3\left(G_{0,-k}T_{0,-r}C_{0,q}\right) \\
&+ \tilde{M}_4\left(T_{0,-k}T_{0,-r}C_{0,q}\right) + \tilde{M}_5\left(G_{0,-k}G_{0,-r}Q_{0,q}\right) + \tilde{M}_6\left(T_{0,-k}G_{0,-r}Q_{0,q}\right) + \tilde{M}_7\left(G_{0,-k}T_{0,-r}Q_{0,q}\right) + \tilde{M}_8\left(T_{0,-k}T_{0,-r}Q_{0,q}\right)\Big], \\
\left[-\!\!\bigcirc\!\!-\right]^{\mathrm{a1}}_{\Gamma^1_{12}} &= -\int \frac{d^dk}{(2\pi)^d}\frac{d\omega}{2\pi} f_{(\mathrm{a1})}(k,k_1,k_2)\Big[\tilde{M}_4\left(G_{0,-k}G_{0,-r}C_{0,q}\right) + \tilde{M}_3\left(T_{0,-k}G_{0,-r}C_{0,q}\right) + \tilde{M}_2\left(G_{0,-k}T_{0,-r}C_{0,q}\right) \\
&+ \tilde{M}_1\left(T_{0,-k}T_{0,-r}C_{0,q}\right) + \tilde{M}_8\left(G_{0,-k}G_{0,-r}Q_{0,q}\right) + \tilde{M}_7\left(T_{0,-k}G_{0,-r}Q_{0,q}\right) + \tilde{M}_6\left(G_{0,-k}T_{0,-r}Q_{0,q}\right) + \tilde{M}_5\left(T_{0,-k}T_{0,-r}Q_{0,q}\right)\Big], \\
\left[-\!\!\bigcirc\!\!-\right]^{\mathrm{a1}}_{\Gamma^1_{22}} &= -\int \frac{d^dk}{(2\pi)^d}\frac{d\omega}{2\pi} f_{(\mathrm{a1})}(k,k_1,k_2)\Big[\tilde{M}_6\left(G_{0,-k}G_{0,-r}C_{0,q}\right) + \tilde{M}_5\left(T_{0,-k}G_{0,-r}C_{0,q}\right) + \tilde{M}_8\left(G_{0,-k}T_{0,-r}C_{0,q}\right) \\
&+ \tilde{M}_7\left(T_{0,-k}T_{0,-r}C_{0,q}\right) + \tilde{M}_2\left(G_{0,-k}G_{0,-r}Q_{0,q}\right) + \tilde{M}_1\left(T_{0,-k}G_{0,-r}Q_{0,q}\right) + \tilde{M}_4\left(G_{0,-k}T_{0,-r}Q_{0,q}\right) + \tilde{M}_3\left(T_{0,-k}T_{0,-r}Q_{0,q}\right)\Big],
\end{aligned}
\tag{S.80}
$$

where the corrections involve sums of products of propagators, with prefactors depending on the allowed interaction vertices. The constants $\tilde{M}_i$, distinct from the symmetric graph corrections Eq. (S.79), are

$$\begin{aligned}
\tilde{M}_1 &= -\frac{1}{2}\left((\Gamma^1_{11})^3 + \Gamma^1_{12}\left(\Gamma^1_{12} + 2\Gamma^1_{22}\right)\Gamma^1_{11} + \Gamma^1_{12}\left(\Gamma^1_{12} + \Gamma^1_{22}\right)^2\right) \\
\tilde{M}_2 &= -\frac{1}{2}\left((\Gamma^1_{12})^3 + (\Gamma^1_{11})^2\Gamma^1_{12} + \left((\Gamma^1_{11})^2 + 2\Gamma^1_{12}\Gamma^1_{11} + 3(\Gamma^1_{12})^2\right)\Gamma^1_{22}\right) \\
\tilde{M}_3 &= -\frac{1}{2}\left(\Gamma^1_{12}\left(\Gamma^1_{11} + \Gamma^1_{12}\right)^2 + 2\Gamma^1_{12}(\Gamma^1_{22})^2 + \left((\Gamma^1_{11})^2 + (\Gamma^1_{12})^2\right)\Gamma^1_{22}\right) \\
\tilde{M}_4 &= -\frac{1}{2}\left((\Gamma^1_{12})^3 + 2\Gamma^1_{22}(\Gamma^1_{12})^2 + (\Gamma^1_{11})^2\Gamma^1_{12} + \Gamma^1_{11}\left(\Gamma^1_{12} + \Gamma^1_{22}\right)^2\right) \\
\tilde{M}_5 &= -\frac{1}{2}\left(2\Gamma^1_{12}(\Gamma^1_{11})^2 + \left((\Gamma^1_{12})^2 + (\Gamma^1_{22})^2\right)\Gamma^1_{11} + \Gamma^1_{12}\left(\Gamma^1_{12} + \Gamma^1_{22}\right)^2\right) \\
\tilde{M}_6 &= -\frac{1}{2}\left((\Gamma^1_{12})^3 + 2\Gamma^1_{11}(\Gamma^1_{12})^2 + (\Gamma^1_{22})^2\Gamma^1_{12} + \left(\Gamma^1_{11} + \Gamma^1_{12}\right)^2\Gamma^1_{22}\right) \\
\tilde{M}_7 &= -\frac{1}{2}\left((\Gamma^1_{12})^3 + 2\Gamma^1_{11}(\Gamma^1_{12})^2 + (\Gamma^1_{22})^2\Gamma^1_{12} + \left(\Gamma^1_{11} + \Gamma^1_{12}\right)^2\Gamma^1_{22}\right) \\
\tilde{M}_8 &= -\frac{1}{2}\left((\Gamma^1_{12})^3 + (\Gamma^1_{22})^2\Gamma^1_{12} + \Gamma^1_{11}\left(3(\Gamma^1_{12})^2 + 2\Gamma^1_{22}\Gamma^1_{12} + (\Gamma^1_{22})^2\right)\right) .
\end{aligned} \tag{S.81}$$

There are 8 distinct products of propagators. Expanding to zeroth order in ω_s, the frequency integral is computed using Cauchy residue theorem and expanded in powers of k_1, k_2. The MSR action transforms as:

$$-\int_{\omega,k}\left[\frac{\Gamma^\alpha_{\beta\gamma}}{2}b^{z+2\chi+\tilde{\xi}+d-2} + -\!\bigcirc\!-\right]\chi_\alpha(\partial_x\theta_\beta)(\partial_x\theta_\gamma) \implies \partial_\ell\Gamma^\alpha_{\beta\gamma} = \left(z + 2\chi + \tilde{\xi} + d - 2 + \frac{[-\!\bigcirc\!-]_{\Gamma^\alpha_{\beta\gamma}}}{\Gamma^\alpha_{\beta\gamma}}\right)\Gamma^\alpha_{\beta\gamma}. \tag{S.82}$$

In the normal mode basis, the non-linear corrections simplify with $\tilde{\Gamma}^1_{11}$ vanishing at one-loop and the other two corrections:

$$\begin{aligned}
[-\!\bigcirc\!-]_{\tilde{\Gamma}^1_{22}} &= K_d\frac{\tilde{\Gamma}^1_{22}\left(\tilde{\Gamma}^1_{11}\tilde{D}_{22} - \tilde{D}_{11}\tilde{\Gamma}^2_{12}\right)\left(\tilde{D}_{11}\tilde{\Gamma}^1_{22}\tilde{\Delta}_{22} - \tilde{\Delta}_{11}\tilde{D}_{22}\tilde{\Gamma}^2_{12}\right)}{d\tilde{D}^2_{11}\tilde{D}^2_{22}\left(\tilde{D}_{11} + \tilde{D}_{22}\right)} \\
[-\!\bigcirc\!-]_{\tilde{\Gamma}^2_{12}} &= K_d\frac{\left(\tilde{\Gamma}^1_{11} - \tilde{\Gamma}^2_{12}\right)\tilde{\Gamma}^2_{12}\left(\tilde{\Delta}_{11}\tilde{D}_{22}\tilde{\Gamma}^2_{12} - \tilde{D}_{11}\tilde{\Gamma}^1_{22}\tilde{\Delta}_{22}\right)}{d\tilde{D}_{11}\tilde{D}_{22}\left(\tilde{D}_{11} + \tilde{D}_{22}\right)^2} .
\end{aligned} \tag{S.83}$$

The structure of these corrections suggest the existence of fixed points, such as the fixed line $X = Y$ where both non-linearities receive no correction. This corresponds to the stable fixed points in Quadrants I and III and the emergence of a fluctuation-dissipation relation and stationary measure.

Flow Equations

The RG flows in the rotated coordinates have already been discussed in Ref. [7] but we present them in our supplementary material for completeness. In total we have 8 parameters in the theory with the RG equations given by

$$\partial_\ell\tilde{\Delta}_{11} = \left[z_1 + 2\bar{\xi} + d - \left(K_d\left((\tilde{\Gamma}^1_{11})^2\tilde{\Delta}^2_{11}\tilde{D}^3_{22} + \tilde{D}^3_{11}(\tilde{\Gamma}^1_{22})^2\tilde{\Delta}^2_{22}\right)/4\tilde{\Delta}_{11}\tilde{D}^3_{11}\tilde{D}^3_{22}\right)\right]\tilde{\Delta}_{11} \tag{S.84a}$$

$$\partial_\ell\tilde{\Delta}_{22} = \left[z_2 + 2\bar{\xi} + d - \left(K_d\left((\tilde{\Gamma}^2_{12})^2\tilde{\Delta}_{11}\tilde{\Delta}_{22}\right)/\tilde{\Delta}_{22}\tilde{D}_{11}\tilde{D}_{22}(\tilde{D}_{11} + \tilde{D}_{22})\right)\right]\tilde{\Delta}_{22} \tag{S.84b}$$

$$\partial_\ell\tilde{D}_{11} = \left[z_1 + \chi_1 + \bar{\xi} + d - 2 + (2-d)\,K_d\left(\left(\tilde{D}^2_{22}\tilde{\Delta}_{11}(\tilde{\Gamma}^1_{11})^2 + \tilde{D}^2_{11}\tilde{\Delta}_{22}\tilde{\Gamma}^1_{22}\tilde{\Gamma}^2_{12}\right)/4d\tilde{D}^3_{11}\tilde{D}^2_{22}\right)\right]\tilde{D}_{11} \tag{S.84c}$$

$$\partial_\ell\tilde{D}_{22} = \left[z_2 + \chi_2 + \bar{\xi} + d - 2 + K_d\left(\tilde{\Gamma}^1_{22}\tilde{\Gamma}^2_{12}\tilde{\Delta}_{22}M_{\tilde{D}_{11},\tilde{D}_2} + (\tilde{\Gamma}^2_{12})^2\tilde{\Delta}_{11}M_{\tilde{D}_2,\tilde{D}_{11}}\right)/\tilde{D}_{22}\right]\tilde{D}_{22} \tag{S.84d}$$

$$\partial_\ell\tilde{\Gamma}^1_{11} = \left[z_1 + 2\chi_1 + \bar{\xi} + d - 2\right]\tilde{\Gamma}^1_{11} \tag{S.84e}$$

$$\partial_\ell\tilde{\Gamma}^1_{22} = \left[z_1 + 2\chi_2 + \bar{\xi} + d - 2 + K_d\left(\left(\tilde{\Gamma}^1_{11}\tilde{D}_{22} - \tilde{D}_{11}\tilde{\Gamma}^2_{12}\right)\left(\tilde{D}_{11}\tilde{\Gamma}^1_{22}\tilde{\Delta}_{22} - \tilde{\Delta}_{11}\tilde{D}_{22}\tilde{\Gamma}^2_{12}\right)/d\tilde{D}^2_{11}\tilde{D}^2_{22}\left(\tilde{D}_{11} + \tilde{D}_{22}\right)\right)\right]\tilde{\Gamma}^1_{22} \tag{S.84f}$$

$$\partial_\ell\tilde{\Gamma}^2_{12} = \left[z_2 + \chi_1 + \chi_2 + \bar{\xi} + d - 2 + K_d\left(\left(\tilde{\Gamma}^1_{11} - \tilde{\Gamma}^2_{12}\right)\left(\tilde{\Delta}_{11}\tilde{D}_{22}\tilde{\Gamma}^2_{12} - \tilde{D}_{11}\tilde{\Gamma}^1_{22}\tilde{\Delta}_{22}\right)/d\tilde{D}_{11}\tilde{D}_{22}\left(\tilde{D}_{11} + \tilde{D}_{22}\right)^2\right)\right]\tilde{\Gamma}^2_{12} \tag{S.84g}$$

and additionally due to the non-renormalisation of the time derivative term we have two exact conditions:

$$\chi_1 + \bar{\xi} + d = 0, \quad \chi_2 + \bar{\xi} + d = 0 \ . \tag{S.85}$$

Owing to the spatial irregularity of white noise, we expect $\bar{\xi} = -3/2$. Up to this point, the corrections Eq. (S.84) are in general dimensions, however we expect that the perturbative RG is only likely to yield good results in $d = 1$. If we consider the set of equations with $z_1 = z_2$ and $\chi_1 = \chi_2$, the flows close under the $\mathbb{R}^4$ space $\{T, X, Y, Z\}$: T is the ratio of diffusion coefficients, X and Y are non-linear cross-couplings, and Z is the KPZ effective non-linearity for the dynamical mode $\tilde{\theta}_1$. The flows are:

$$\begin{aligned}
\frac{d}{d\ell}T &= -\frac{Z}{\pi}\left(T + XY + \frac{2X((T-3)X - 3TY + Y)}{(1+T)^2}\right) \\
\frac{d}{d\ell}X &= -\frac{4Z}{\pi}\frac{X(X-1)(X-Y)}{(1+T)^2} \\
\frac{d}{d\ell}Y &= \frac{Z}{\pi}\frac{Y(X-Y)\left(2(5T+1)X + (1+T)^2Y - 4T(1+T)\right)}{T(1+T)^2} \\
\frac{d}{d\ell}Z &= Z\left(\frac{Z(Y(Y-3X) - 2T)}{\pi T} + 1\right) ,
\end{aligned} \tag{S.86}$$

where all flows feature a multiplicative factor of Z. Solving these equations becomes an initial value problem involving evolving the bare parameters at $\ell = 0$ (initial RG time) to $\ell \to \infty$ which captures the dynamics of the coarse grained theory. The flows for $\{X, Y, Z\}$ are self-generated i.e. $\partial_\ell X = 0$ if X = 0. The fixed points in the adimensionalised RG flows can be found by setting the RHS of Eq. (S.86) to vanish. For bare parameters lying in Quadrants I and III, the flows predict a line of fixed points along $X = Y$ as shown in FIG. 2 enforcing $\chi = 1/2$. The flows for all interaction vertices Γ vanish along the FDR and additionally $\chi = 1/2$, giving rise to KPZ scaling $z = 3/2$ for both modes. For distinct initial points, the flows intersect the FDR line at different values of X, determining the fixed points T^* and Z^*, where we introduce the asterisk notation to denote the RG fixed point as $\ell \to \infty$. In the recent posting Ref. [8], D. Roy et al. propose that this corresponds to a smooth foliation of universality classes for a two-dimensional surface in the larger parametric space

Along the FDR, there is an emergent stationary measure and this results in the non-renormalisation of the same time two-point correlation functions. The fixed point in the adimensionalised RG flows in Quadrant I and III is $X = Y$. This gives an algebraic condition for the stationary values of T^* and Z^*. Solving for T^* in terms of the fixed point X^* gives

$$T(X^*) = \frac{1}{2}\left(-1 - (X^*)^2 + \sqrt{(1+(X^*)^2)^2 + 12(X^*)^2}\right) \tag{S.87}$$

as plotted in FIG.S2(a). As X^* goes to zero along the FDR, the fixed point coincides with T^* vanishing. The parameter T controls the relative relaxation of the modes suppressing height fluctuations. This also reveals a breakdown in the scaling hypothesis as we approach the exceptional point where there is a KPZ mode decoupled to a EW mode. At intermediate times and lengthscales, the $\mathbb{Z}_2$ basis rotates distinct scaling modes with $z_1 \neq z_2$ into one another. This behaviour is hinted at in the numerical simulation at $X = 1/2$, $Y = 1/2$ in Section D where the fluctuation distribution for $\tilde{\theta}_2$ is more Gaussian with smaller kurtosis, suggesting the need for better methods to probe this extremal point. Moreover, the flows can be solved to calculate the ratio of the same-time two point correlation functions

$$\frac{\tilde{C}_{22}}{\tilde{C}_{11}} = \frac{\tilde{\Delta}_{22}}{\tilde{D}_{22}}\frac{\tilde{D}_{11}}{\tilde{\Delta}_{11}} \tag{S.88}$$

revealing that the ratio reaches a fixed point. The fixed point can be used to explain differences in the heights of the two-point correlation function. The general structure which is revealed in FIG. S2(c)-(d) is that the ratio is positive when the initial bare values are above the FDR line and negative when the initial bare values start from below the FDR.

There are two distinct behaviours along the Cole-Hopf line. When $Y > 0$, independent of the initial T we flow to a point where $T^* = 1$, $X^* = Y^* = 1$ where FDR is satisfied. Consequently, the renormalised parameters for the noise and interaction vertices satisfy $(\tilde{\Gamma}^{1*}_{22}\Delta^*_{22})/(\tilde{\Gamma}^{1*}_{11}\Delta^*_{11}) = 1$. At the fixed point there exists a transformation, $\hat{\theta}^\alpha = s^\alpha_\beta \tilde{\theta}^\beta$ with

$$s = \begin{pmatrix} \tilde{\Gamma}^{1*}_{11} & (\tilde{\Gamma}^{1*}_{11}\tilde{\Gamma}^{1*}_{22})^{1/2} \\ \tilde{\Gamma}^{1*}_{11} & -(\tilde{\Gamma}^{1*}_{11}\tilde{\Gamma}^{1*}_{22})^{1/2} \end{pmatrix} \tag{S.89}$$

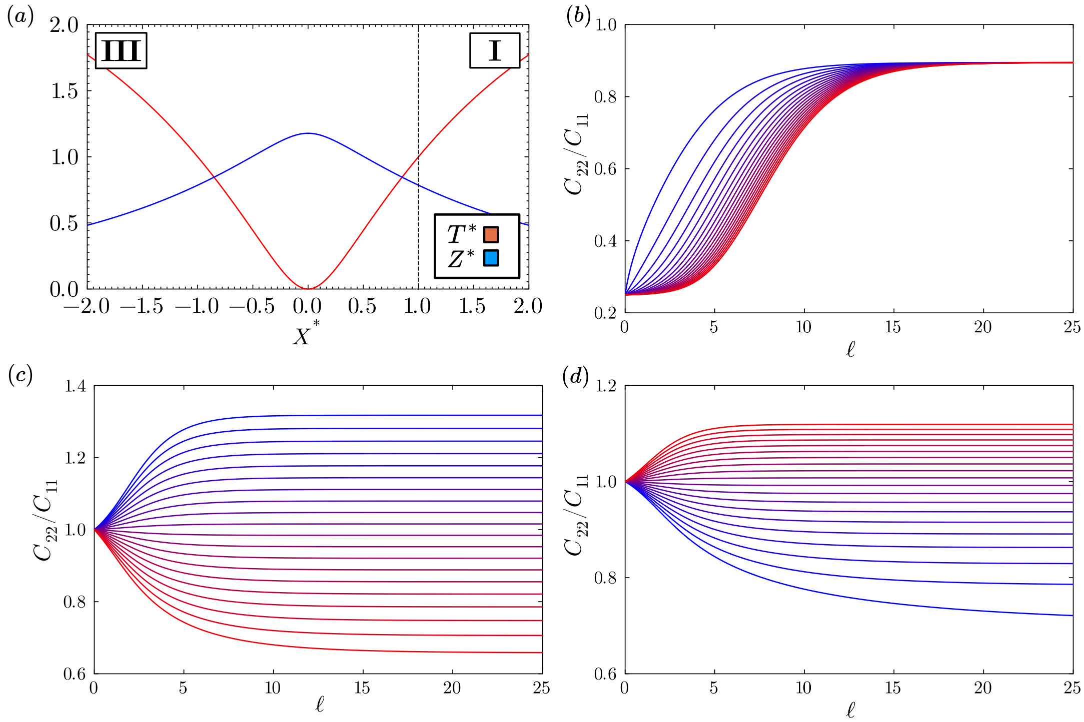

FIG. S2. **Fixed Point Structure of Flows in Stable Quadrants** : (a) From Eq. (S.86), the fixed points of the flows in Quadrants I and III lie on the FDR line $X = Y$. The intersection of the flow determines the fixed point structure for both T and Y. The fixed points T^* and Z^* are shown in red and blue respectively. (b-d) We consider the flows of $\tilde{C}_{22}/\tilde{C}_{11} = (\tilde{\Delta}_{22}\tilde{D}_{11})/(\tilde{\Delta}_{11}\tilde{D}_{22})$ for lines in the (X, Y)-plane. (b) Starting with $\tilde{C}_{22}/\tilde{C}_{11} = 0.25$ along the Cole-Hopf line with $X = 1$, $Y = 0.5$ but with $\tilde{D}_{11} = \tilde{\Delta}_{11} = \tilde{D}_{22} = s$ and $\tilde{\Delta}_{22} = 0.25s$ where s is varied from 0 (blue) to 4 (red) in even intervals, the fixed point is shown to be a function of the initial ratios $\tilde{C}_{11}$ and $\tilde{C}_{22}$ only. For (c) and (d), we look at non-universal flows of $\tilde{C}_{22}/\tilde{C}_{11}$ taking the bare parameters $\tilde{\Delta}_{11} = \tilde{D}_{11} = \tilde{\Delta}_{22} = \tilde{D}_{22} = 1$ and $\tilde{\Gamma}^1_{11} = -1.0$. (c) With $X = 1$ along the Cole-Hopf line, varying $Y \in \{0.7, 1.3\}$ in even steps reveals that $\tilde{C}_{22}/\tilde{C}_{11} > 1$ for flows starting below the FDR line (shown by blue) and $\tilde{C}_{22}/\tilde{C}_{11} < 1$ for flows starting above the FDR line (shown in red). (d) With $Y = 1$, varying $X \in \{0.85, 1.15\}$ in even steps reveals that the same behaviour of $\tilde{C}_{22}/\tilde{C}_{11}$ above and below the line.

where the equations decouple symmetrically

$$
\begin{aligned}
\partial_t \hat{\theta}_1 &= \tilde{D}^*_{11}\partial_x^2\hat{\theta}_1 + \frac{1}{2}(\partial_x\hat{\theta}_1)^2 + \tilde{\Gamma}^{1*}_{11}\sqrt{2\tilde{\Delta}^*_{11}}\,(\zeta_1 + \zeta_2) \\
\partial_t \hat{\theta}_2 &= \tilde{D}^*_{11}\partial_x^2\hat{\theta}_2 + \frac{1}{2}(\partial_x\hat{\theta}_2)^2 + \tilde{\Gamma}^{1*}_{11}\sqrt{2\tilde{\Delta}^*_{11}}\,(\zeta_1 - \zeta_2)\,.
\end{aligned}
\tag{S.90}
$$

In the decoupled coordinates, there is a definite scaling hypothesis for the two-point correlation functions and coordinate transformations come from rotating KPZ modes into one another. Experimentally, measurements are made in the original $\mathbb{Z}_2$ coordinates. Therefore, analytical forms of the distributions in the physical coordinates requires the inverse of the normal mode transformation in Eq. (S.89). Experimentally, this means that one-point measurements in the original $\mathbb{Z}_2$-coordinates will deviate from Tracy-Widom distributions if $\tilde{\Gamma}^{1*}_{22} \neq \tilde{\Gamma}^{1*}_{11}$. This poses a slight complication in matching the distribution of fluctuations in coupled spinor condensates.

SUPPLEMENTARY NOTE 4 : DIRECT SIMULATIONS OF QUADRANT I

The analytical discussion relies on the accurate description of the scaling by perturbative RG around the decoupled point $(X, Y) = (1, 1)$. However, it does not rule out the possibility of non-perturbative effects altering the scalings. To provide a more comprehensive view on the RG results, we perform direct simulations of the coupled KPZ equations in Quadrant I in the $\mathbb{Z}_2$ coordinate system. We employ the forward Euler-Maruyama method to directly integrate the stochastic fields θ_{i,t_i}. The finite difference discretisation is crucial in ensuring correct behaviour, especially in preventing instabilities from large height differences between neighbouring lattice points $\Delta h > h_c \sim O\left(\Delta\Gamma^2/D^3\right)^{-1/2}$. The discretised coupled KPZ equation can be written as a system of stochastic ODEs, with two component degrees of freedom α at each lattice point

$$\theta^\alpha_{t_{i+1}} = \theta^\alpha_{t_i} + \left[D^\alpha_\beta L^\beta[\theta] + \Gamma^\alpha_{\beta\gamma} N^\beta[\theta] N^\gamma[\theta]\right] \Delta t + \Delta W^\alpha_{t_i}. \tag{S.91}$$

where the discretised Laplacian operator is

$$L[\theta^\alpha_i] = (\theta^\alpha_{t_i,x+1} - 2\theta^\alpha_{t_i,x} + \theta^\alpha_{t_i,x-1})/2\Delta x\ . \tag{S.92}$$

The fields are integrated from flat initial conditions $\theta^\alpha(t=0) = 0$ to $t = 800$ with a time spacing $\Delta t = 0.01$. The noise term ΔW_{t_i} follows a centred Gaussian distribution with increments $\Delta W^\alpha_{t_i} = W^\alpha_{t_i} - W^\alpha_{t_{i-1}} \sim N(0, 2\tilde{\Delta}_{\alpha\alpha}\Delta t)$, which reproduce the covariance matrix. The white noise process is expressed as the sum of two independent processes $\Delta W^\alpha_{t_i} = \sqrt{12\Delta t} R_{1,t_i}\sqrt{2\tilde{\sigma}_1} + \sqrt{12\Delta t} R_{2,t_i}\sqrt{2\tilde{\sigma}_2}$ where $\tilde{\sigma}_i = (\Delta_{11} \pm \sqrt{\Delta^2_{11} - \Delta^2_{12}})/2$ and is approximated from sampling a centered uniform distribution $R_{i,t_i} \sim U([-0.5, 0.5])$. The noise discretisation is common in numerics of stochastic equations as a Wiener process can be generated as a limiting process of a random walk with equivalent first and second moments. For the non-linear operators, we define the discretised derivative N

$$N^\alpha[\theta_j] = \left(\frac{\theta^\alpha_{j+1} - \theta^\alpha_{j-1}}{2\Delta x}\right). \tag{S.93}$$

We set all $D_{11} = \Delta_{11} = 1$ and $\Gamma^1_{11} = -1$, thus $Z_0 \sim 1$ which limits instabilities in the height surface while still ensuring a crossover to KPZ scaling. There were two primary goals: (a) to characterise the exponents for increasing system sizes, verifying convergence to $\chi = 1/2$ and $z = 3/2$ for both dynamical modes in rotated and unrotated coordinates initialised away from the $X = Y$ line, and (b) to characterise the distribution of fluctuations on the FDR manifold X=Y and the Cole-Hopf line. This numerical investigation allows us to test and verify the scaling predictions from the RG analysis, providing insights into both the perturbative and non-perturbative behavior of the coupled KPZ system.

Dynamical Exponents

To classify the dynamical exponents in Quadrant I, we investigate how the scaling behaves in the long system size and time limit. The length of the system is varied across $\{2^8, 2^{12}, 2^{16}, 2^{20}\}$, and we analyse the finite size convergence of the roughness α, growth β, and dynamical z exponents. We consider two points I.A. and I.B., shown in TABLE S1, located away from the FDR line $X = Y$ and Cole-Hopf line $X = 1$. In the single-component theory, the surface roughness

$$W_\alpha(t) = \langle\overline{(\theta_\alpha)^2} - \overline{\theta_\alpha}^2\rangle \sim t^{2\beta}, \quad t \ll L^z \tag{S.94}$$

can be fitted to extract the growth exponent β, demonstrating a crossover from EW $\beta = 1/4$ to KPZ $\beta = 1/3$ in the long wavelength limit. While simulations tend to underestimate β in the growth phase, the values are within expected error margins. This underestimation can be attributed to the EW to KPZ crossover. The scaling of the two-point same-time correlation function

$$\hat{C}_{\alpha\beta}(|x - x'|) = \langle(\theta_\alpha(x + x') - \theta_\beta(x))^2\rangle = C_{\alpha\beta}|x - x'|^{2\chi}. \tag{S.95}$$

can be fitted to extract the roughness exponent α from which the dynamical exponent is fixed by their ratio. The fitted values for $L = 2^{20}$ are plotted in FIG. S3. The full list of initial values and fitted values is contained in TABLE S1. For points initialised on the FDR line, the correlation functions satisfy $\tilde{C}_{11} = \tilde{C}_{22} \approx 1$, which aligns with the same-time correlations remaining their bare values under RG strictly imposed by emergent Ward-Takahashi identities. This verifies that the FDR line is stationary under RG. Away from the FDR line, such as at points I.A. and I.B., the correlations flow to a non-unity value, suggesting that the correlation functions are renormalised as predicted by the flows in FIG. (S2).

Distributions of Fluctuations

The distributions of fluctuations along the Cole-Hopf line highlight that the RG flow decouples the KPZ equations, leading to fluctuations that are the sum and difference of TW-GOE distributions. This is discussed in the main paper

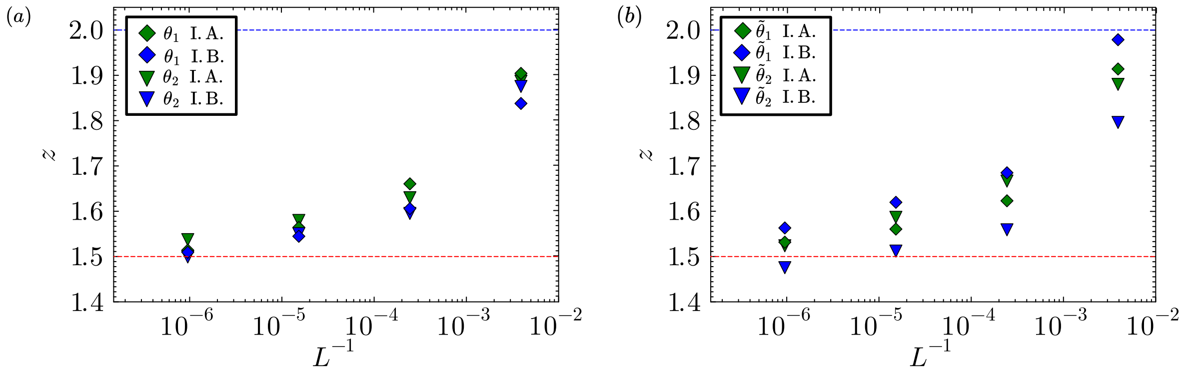

FIG. S3. **Finite Scaling Analysis of Exponents** : The dynamical exponent z plotted against $1/L$ where Subfigure (a) shows the finite scaling analysis for the unrotated $\mathbb{Z}_2$ coordinates and Subfigure (b) shows convergence in the normal mode basis. In both cases there is the expected crossover as predicted by the RG flow from $z = 2$ Edwards-Wilkinson behaviour to $z = 3/2$ KPZ scaling.

	RG I.C.				**Unrotated θ_1**					**Rotated $\tilde{\theta}_1$**					**Rotated $\tilde{\theta}_2$**				
	X	Y	T	W	v_∞	$\tilde{M}_\infty$	β	α	C_{11}	v_∞	$\tilde{M}_\infty$	β	α	$\tilde{C}_{11}$	v_∞	$\tilde{M}_\infty$	β	α	$\tilde{C}_{22}$
CH	1.0	2.0	0.5	2.0	-0.200	0.546	0.316	0.484	1.048	-0.283	0.449	0.281	0.467	1.026	0.000	0.649	0.281	0.498	1.073
FDR	1.0	1.0	1.0	1.0	-0.248	0.512	0.298	0.466	1.042	-0.35	0.512	0.298	0.466	1.042	0.000	0.512	0.298	0.466	1.042
FDR	2.0	2.0	1.0	1.0	-0.212	0.518	0.298	0.467	1.040	-0.30	0.469	0.29	0.465	1.046	0.000	0.569	0.290	0.468	1.035
FDR	0.5	0.5	1.0	1.0	-0.297	0.502	0.306	0.476	1.027	-0.42	0.609	0.319	0.478	1.02	0.000	0.403	0.319	0.475	1.034
I.A.	1.07	0.73	1.11	0.82	-0.242	0.51	0.306	0.472	1.041	-0.342	0.545	0.295	0.464	1.195	0.000	0.475	0.295	0.483	0.889
I.B.	0.98	2.18	1.63	0.75	-0.324	0.582	0.309	0.477	1.102	-0.458	0.882	0.309	0.474	1.483	-0.001	0.327	0.309	0.484	0.721

TABLE S1. **Fitted Parameters from Numerical Simulations** : Scalings for initial bare parameters in Quadrant I. v_∞ and $\tilde{M}_\infty$ refer to the fitted values at $t = \infty$ for $L = 2^{20}$. Static properties such as $C_{\alpha\beta}$ are calculated at time shot $t = 800$.

in FIG.5. This is evident from the simulated distributions agreeing with the expected distributions in yellow, as well as the moments approaching their expected values over long times. For $(X, Y) = (1/2, 1/2)$, the rotated coordinates $\tilde{\theta}_2$ have less kurtosis and is closer to a Gaussian. This smooth crossover along the FDR line from TW-GOE to Gaussian is expected, as at $X = 0$ the equations are decoupled with a KPZ mode and an Edwards-Wilkinson mode. This behaviour should be apparent at finite time and finite system-size, however whether it remains in the long-time limit is not explored. At point $(X, Y) = (2, 2)$, $\tilde{\theta}_1$ displays a longer tail to the right indicating the reverse effect. These results clearly showcase the smooth crossover effect as the system moves across the FDR line, with distinct fluctuation behaviors emerging in the regions.

SUPPLEMENTARY NOTE 5 : SPACETIME VORTEX DOMINATED PHASE

As the intercomponent interaction v_c is tuned from the decoupled point $(X, Y) = (1, 1)$ into Quadrant IV where the theory is non-hyperbolic, the coupled KPZ equations generates large spatial fluctuations $\theta(x_i, t_j) - \theta(x_{i+1}, t_j) > 2\pi$ in the unwrapped phase. Physically, the phase is a compact variable and the large height fluctuations give rise to a spacetime vortex (STV) dominated phase. This instability arises from the balance between the diffusion constant, acting as viscosity, smoothing out fluctuations, and the non-linear term driving the system into a rough geometry. The KPZ theory describes this rough geometry, and the crossover rate from flat to rough geometry is related to the size of the restorative diffusion term. The charge of the vortex c^* is

$$c^* = \frac{1}{2\pi}\left[\mathcal{U}(\theta_{i,j+1}, \theta_{i+1,j}) + \mathcal{U}(\theta_{i-1,j}, \theta_{i,j+1}) + \mathcal{U}(\theta_{i,j-1}, \theta_{i-1,j}) + \mathcal{U}(\theta_{i+1,j}, \theta_{i,j-1})\right] \tag{S.96}$$

where $\mathcal{U}$ calculates the unravelled phase difference between two points. In systems with $U(1) \times U(1)$ symmetry, the elementary topological excitations are half-vortices in either component in the unrotated $\mathbb{Z}_2$ theory.

We simulate the SCGLE Eq. (1) in the low-noise regime with $\gamma_T = 0.1$ and time step $dt = 0.01$ up to $t_{\text{tot}} = 10^5$ using a system size $L_x = 2048$. The total time is much larger than the saturation time L_{sat} which is proportional to

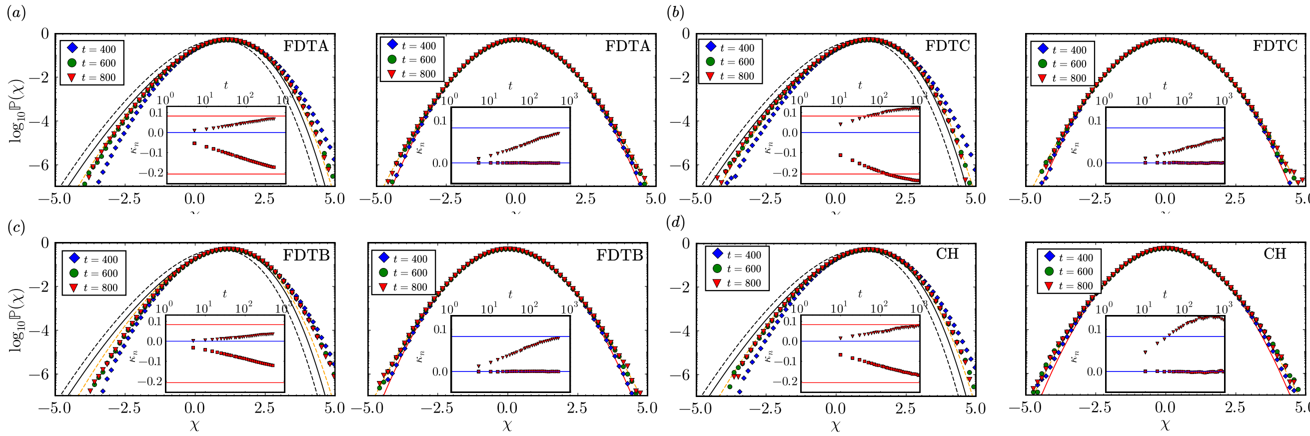

FIG. S4. **Further Distribution of Fluctuations in Quadrant I** : Distribution of fluctuations for $\tilde{\theta}_1$ and $\tilde{\theta}_2$ on the left and right respectively for initial bare parameter values in Quadrant I. The subfigures within each graph show the convergence of the moments of the distributions which are the skewness and kurtosis. (a) FDTA corresponds to $(X, Y) = (1, 1)$ at the decoupled point. (b) FDTC corresponds to $(X, Y) = (1/2, 1/2)$. (c) FDTB corresponds to $(X, Y) = (2, 2)$. (d) CH correspondings $(X, Y) = (1, 2)$. All parameters and relevant scalings can be found in Table S1.

L_x^z where z is the KPZ dynamical exponent. Tuning $\tilde{v}_c$ defines a line $\gamma : [-1.2, 0] \to \mathbb{R}^2$ for $\tilde{v}_c \mapsto (X, Y)$ as shown in FIG. 4(a). Parameters are set $v_d = 0$, $k_d = u_d = \mu_d = 1$ and $k_c = 3$, $u_c = 1.5$. μ_c is determined by solving the consistency relation $\mu_c = -(u_c + v_c)$ with the density fixed $\rho = 1$. The chosen parameters mean that time t and space x are in units of μ_d^{-1} and $\sqrt{k_d}$ respectively. Setting $v_d = 0$ the mapping to (X, Y) is:

$$
\begin{aligned}
X &= \frac{2(\mathcal{R}(k) - \mathcal{R}(u))}{\mathcal{R}(k)\tilde{v}_c + \mathcal{R}(k) - \mathcal{R}(u)} - 1 \\
Y &= \frac{\left(\mathcal{R}(u)^2 + (\tilde{v}_c - 1)^2\right)\left(\mathcal{R}(k)\mathcal{R}(u) + \tilde{v}_c + 1\right)}{\left(\mathcal{R}(u)^2 + (\tilde{v}_c + 1)^2\right)\left(\mathcal{R}(k)\mathcal{R}(u) - \tilde{v}_c + 1\right)}
\end{aligned}
\tag{S.97}
$$

which converges to $(1, 1)$ in the decoupled limit $\tilde{v}_c \to 0$. The time-unravelled phase is analysed across $L_t = 2000$ time sampling points. Consequently, the time spacing on the spacetime lattice is $t_{\text{tot}}/L_t = 50$. The spatial unit is $\Delta x = 1$. We have two measures for the onset of the STV phase, the probability of vortices on the spacetime lattice and the autocorrelation function. We define the autocorrelation function

$$
\Delta_\alpha(t_1 - t_2) = \overline{\langle(\theta_\alpha(t_1) - \theta_\alpha(t_2))^2\rangle} - \overline{\langle(\theta_\alpha(t_1) - \theta_\alpha(t_2))\rangle}^2 \sim |t_1 - t_2|^{2\beta}. \tag{S.98}
$$

as time-time correlations of locally defined points on the lattice. $\langle\cdot\rangle$ indicates averaging over trajectories and $\overline{\cdot}$ as a spatial average over lattice points. To ensure that we are probing long-time dynamics, we evolve the simulation to $t_2 = 50000$ in the saturation regime L_x^z, thus the autocorrelation function in FIG. 4(a-c) shows the systems between $t = 5 \times 10^4$ to $t = 10^5$. For KPZ systems, starting from an flat initial conditions, we expect to see a crossover from Edwards-Wilkinson scaling with $\beta = 1/4$ to $\beta = 1/3$ for large system sizes and large times. However, in the STV dominated phase, the growth exponent is $\beta = 1/2$ indicating a departure from the expected scaling. The other measure is the vortex probability $\mathcal{P}_v$ which is defined as the ratio of the number of vortices in each component N_v to the total number of spacetime lattice points $N_{v_i}/(L_t \times L_x)$. We use periodic boundary conditions and expect that the solution is translationally invariant. The probability of a vortex across the whole spacetime lattice features a smooth crossover from a suppressed vortex phase in Quadrant I to a vortex dominated phase in Quadrant IV.

SUPPLEMENTARY NOTE 6 : CONNECTION TO EXCITON-POLARITON EXPERIMENT

In many theoretical studies, there can be a preference to start with the generalised Gross-Pitaevskii Equations since the polariton fields ψ_i can interact with excitons in the semiconductor cavity. Since both descriptions describe a non-equilibrium condensate with $U(1) \times U(1)$ symmetry, they give rise to equivalent low-energy theories described by coupled KPZ equations. However they can differ on the exact bare values of parameters in the multicomponent KPZ.

To connect these results better to experiment, we also present a derivation of the parameters for the multicomponent KPZ equations and interpret the parameter space sweeped through by current experiments. The gGPE equations in multicomponent form are given by the rate equations of multicomponent excitons with density $n_{R,1}$, $n_{R,2}$ coupled to the two component condensate ψ_1, ψ_2 with dynamics

$$\begin{aligned}
\partial_t n_{R,1} &= P - (\gamma_R + R_1|\psi_1|^2 + R_2|\psi_2|^2) n_{R,2} \\
\partial_t n_{R,2} &= P - (\gamma_R + R_1|\psi_2|^2 + R_2|\psi_1|^2) n_{R,1} \\
i\hbar\partial_t\psi_1 &= \Big[E[\hat{k}] - \tfrac{i\hbar}{2}\gamma(\hat{k}) + g_1|\psi_1|^2 + g_2|\psi_2|^2 + 2g_{R,1}n_{R,1} + 2g_{R,2}n_{R,2} + \tfrac{i\hbar}{2}\left(R_1 n_{R,1} + R_2 n_{R,2}\right)\Big]\psi_1 + \hbar\xi_1 \\
i\hbar\partial_t\psi_2 &= \Big[E[\hat{k}] - \tfrac{i\hbar}{2}\gamma(\hat{k}) + g_1|\psi_2|^2 + g_2|\psi_1|^2 + 2g_{R,1}n_{R,2} + 2g_{R,2}n_{R,1} + \tfrac{i\hbar}{2}\left(R_1 n_{R,2} + R_2 n_{R,1}\right)\Big]\psi_2 + \hbar\xi_2
\end{aligned} \tag{S.99}$$

where we have followed the convention in previous 1D experiments [9]. We have also imposed a $\mathbb{Z}_2$ symmetry in the pumping and in the bath parameters in line with the rest of the paper. This is a generalisation to multicomponents where we assume that the dynamics of the two exciton species become correlated due to the spinor nature of the lower polariton band. In the general form, the blueshift due to the interactions with the excitons becomes multicomponent and the stimulated emission also inherits this structure with terms

$$g_R n_R \mapsto g_{R,1}n_{R,1} + g_{R,2}n_{R,2}\,,\ R\,n_R \mapsto R_1 n_{R,1} + R_2 n_{R,2}\,. \tag{S.100}$$

In Eq. (S.99), the noise is a diagonal Gaussian white noise with covariance $2\xi_0, \delta(t-t')\,\delta(x-x')$ with $\xi_0 = (R_1 n_{R,1} + R_2 n_{R,2})/2$ as predicted by Truncated-Wigner. The dispersion is taken as a quadratic with $E[\hat{k}] = E_0 - \hbar^2\partial_x^2/2m$ and the polariton linewidth $\gamma(\hat{k})$ is taken as $\gamma(k \simeq 0) \simeq \gamma_0 - \gamma_2\partial_x^2$ where in both cases we have explicitly written out the momentum operator as a real space derivative. The process of adiabatically eliminating the gapped fields around the mean field solution with $\psi_i(x,t) = \sqrt{\rho_i(x,t)}\exp[i(\theta_i(x,t) - \overline{\omega}_0 t)]$ can be done in an analogous way to Ref. [9] where the emission linewidth becomes

$$\omega_0 = 2\tfrac{\overline{g}_R\gamma_0}{\hbar\overline{R}}\left[2 + (p-1)\tfrac{\overline{g}}{\overline{g}_R}\tfrac{\gamma_R}{\gamma_0}\right] \tag{S.101}$$

with $\overline{R} = R_1 + R_2$, $\overline{g} = g_1 + g_2$, $\overline{g}_R = g_{R,1} + g_{R,2}$. Additionally we define the difference between the intercomponent and intracomponent as $\Delta R = R_1 - R_2$, $\Delta g = g_1 - g_2$, $\Delta g_R = g_{R,1} - g_{R,2}$. Solving for small fluctuations in $\theta_{1,2}$ and ignoring all derivatives of gapped quantities gives a multicomponent KPZ equation with viscosity parameters for the diffusion matrices

$$D_{11} = D_{22} = \frac{\gamma_2}{2} - \left[\overline{u}\frac{\overline{g}_R}{\hbar\overline{R}} + \Delta u\frac{\Delta g_R}{\hbar\Delta R} + \frac{\Delta g}{\hbar\Delta R}\frac{\gamma_R}{\gamma_0}\left(1 - \frac{\overline{R}}{\Delta R}\right)\right]\frac{\hbar}{2m} \tag{S.102a}$$

$$D_{12} = D_{21} = -\left[\overline{u}\frac{\overline{g}_R}{\hbar\overline{R}} - \Delta u\frac{\Delta g_R}{\hbar\Delta R} - \frac{\Delta g}{\hbar\Delta R}\frac{\gamma_R}{\gamma_0}\left(1 - \frac{\overline{R}}{\Delta R}\right)\right]\frac{\hbar}{2m} \tag{S.102b}$$

where we additionally define

$$\overline{u} = 2 - p\frac{\overline{g}}{\overline{g}_R}\frac{\gamma_R}{\gamma_0}\,,\ \Delta u = 2 - p\frac{\Delta g}{\Delta g_R}\frac{\gamma_R}{\gamma_0} \tag{S.103}$$

and this reduces to the single-component KPZ parameters without off-diagonal D_{12} when cross-couplings vanish, as presented in Ref. [9]. The non-linear couplings are

$$\Gamma^1_{11} = \Gamma^2_{22} = -2\left[\frac{\hbar}{2m} + \frac{1}{2}\left(\overline{u}\frac{\overline{g}_R}{\hbar\overline{R}} + \Delta u\frac{\Delta g_R}{\hbar\Delta R} + \frac{\Delta g}{\hbar\Delta R}\frac{\gamma_R}{\gamma_0}\left(1 - \frac{\overline{R}}{\Delta R}\right)\right)\gamma_2\right] \tag{S.104a}$$

$$\Gamma^1_{22} = \Gamma^2_{11} = -\left[\overline{u}\frac{\overline{g}_R}{\hbar\overline{R}} - \Delta u\frac{\Delta g_R}{\hbar\Delta R} - \frac{\Delta g}{\hbar\Delta R}\frac{\gamma_R}{\gamma_0}\left(1 - \frac{\overline{R}}{\Delta R}\right)\right]\gamma_2 \tag{S.104b}$$

and $\Gamma^1_{12} = \Gamma^1_{21} = \Gamma^2_{12} = \Gamma^2_{21}$. The noise terms are

$$\Delta_{11} = \Delta_{22} = \frac{\xi}{2\rho_0}\left[1 + 2\left[\left(\overline{u}\frac{\overline{g}_R}{\hbar\overline{R}}\right)^2 + \left(\Delta u\frac{\Delta g_R}{\hbar\Delta R} + \frac{\Delta g}{\hbar\Delta R}\frac{\gamma_R}{\gamma_0}\left(1 - \frac{\overline{R}}{\Delta R}\right)\right)^2\right]\right] \tag{S.105a}$$

$$\Delta_{12} = \Delta_{21} = \frac{\xi}{\rho_0}\left[\left(\overline{u}\frac{\overline{g}_R}{\hbar\overline{R}}\right)^2 - \left(\Delta u\frac{\Delta g_R}{\hbar\Delta R} + \frac{\Delta g}{\hbar\Delta R}\frac{\gamma_R}{\gamma_0}\left(1 - \frac{\overline{R}}{\Delta R}\right)\right)^2\right] \tag{S.105b}$$

where ρ_0 is the mean field density for both components. These are a $\mathbb{Z}_2$ generalisation of the coupled equations but reduce to the standard single-component case when there are two uncorrelated components. In this particular experimental setup, the real scattering interaction between polaritons is orders of magnitude smaller than the polariton blueshift. Additionally, we take $g_{R,2} = 0$ so that there is no blueshift due to interactions with the other components reservoir. However we assume that the scattering rate R_2 does not completely vanish and can be written in terms $\tilde{R} = R_2/R_1$ in units of R_1. In this instance, we can consider where the theory maps to in the (X, Y)-plane to understand the relevance of the cross-coupling interaction. There are two parameters which determine the position in the parametric space which are shown in FIG. S5: $R(k) = k_d/k_c = (\hbar\gamma_2)/(\hbar^2/m)$. In this case $\hbar\gamma_2 = 1.6 \times 10^4\, \mu\, eV.\mu m^2$ and $m_{LP} = -3.3 \times 10^{-6}\, m_e$ giving $\hbar^2/m_p \approx -1.15 \times 10^4\, \mu\, eV.\mu m^2$ such that $R(k) \approx -1.4$; and $R(u) = u_d/u_c$ where $u_d = R_1 = 8.8 \times 10^{-4} \mu m.ps^{-1}$ and $u_c = g_R$ with

$$g_R = \frac{1}{2}\frac{\mu_{th} R}{\gamma_0} \approx 1.3 \times 10^{-2}\, \mu m.ps^{-1} \tag{S.106}$$

giving $R(u) \approx 0.06$. This results in a parametric curve depending on three parameters

$$(X(\tilde{R}, R(k), R(u)), Y(\tilde{R}, R(k), R(u)) \tag{S.107}$$

with limiting values

$$\lim_{R(u)\to 0} (X, Y) = (\tfrac{1+\tilde{R}}{1-\tilde{R}}, \tfrac{1+\tilde{R}}{1-\tilde{R}}) \tag{S.108a}$$

$$\lim_{R(k)\to 0} (X, Y) = (1,\, Y(\tilde{R}, 0, R(u)) \tag{S.108b}$$

such that in the limit that $k_d \to 0$ we are on the Cole-Hopf line with a decoupling transformation whereas in the limit that $R(u) \to 0$ we lie on the line of fixed points defining the emergence fluctuation dissipation relation. For particular combinations of $R(u)$, $R(k)$ we can explore the entire parametric space.

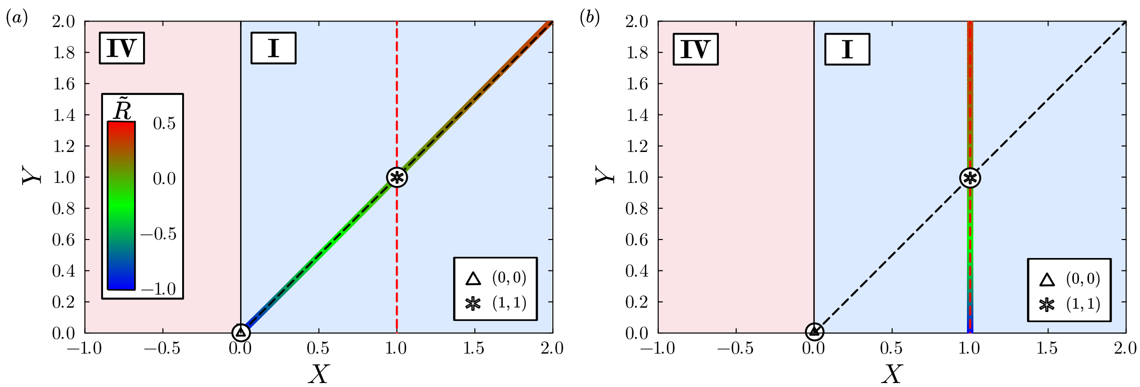

FIG. S5. **Parametric Space for gGPE in Different Limits** : The mapping from the microscopic theory to the parametric space (X, Y) has two important limits: (a) In Eq. (S.108a) where $|R(k)| \gg |R(u)|$ which is the case for the experimental observation of KPZ; and (b) In Eq. (S.108b) where the diffusion constant vanishes and we map onto the Cole-Hopf line. Tuning the coupling parameters between the two multicomponent system traces out lines in the plane with the decoupled KPZ point at $(1, 1)$. In this case, the tuning parameter is the relevant strength of the cross-scattering of the polaritons with excitons denoted by $\tilde{R}$.

SUPPLEMENTARY REFERENCES

[1] Sieberer, L. M., Huber, S. D., Altman, E. & Diehl, S. Nonequilibrium functional renormalization for driven-dissipative Bose-Einstein condensation. *Phys. Rev. B* **89**, 134310 (2014).

[2] He, L. & Diehl, S. Miscible–immiscible transition and nonequilibrium scaling in two-component driven open condensate wires. *New J. Phys.* **19**, 115012 (2017).

[3] Sieberer, L. M., Buchhold, M. & Diehl, S. Keldysh field theory for driven open quantum systems. *Rep. Prog. Phys.* **79**, 096001 (2016).

[4] Prähofer, M. & Spohn, H. Scale invariance of the PNG droplet and the Airy process. *J. Stat. Phys.* **108**, 1071–1106 (2002).
[5] Quastel, J. & Spohn, H. The one-dimensional KPZ equation and its universality class. *J. Stat. Phys.* **160**, 965–984 (2015).
[6] Canet, L., Chat, H., Delamotte, B. & Wschebor, N. Nonperturbative renormalization group for the Kardar-Parisi-Zhang equation: General framework and first applications. *Phys. Rev. E* **84**, 061128 (2011).
[7] Ertaş, D. & Kardar, M. Dynamic relaxation of drifting polymers: A phenomenological approach. *Phys. Rev. E* **48**, 1228–1245 (1993).
[8] Roy, D., Dhar, A., Kulkarni, M. & Spohn, H. Fixed points and universality classes in coupled Kardar-Parisi-Zhang equations. *arXiv preprint* arXiv:2504.04162 (2025).
[9] Fontaine, Q. *et al.* Kardar–Parisi–Zhang universality in a one-dimensional polariton condensatep. *Nature* **608**, 687–691 (2022).